Changes in cloud and aerosol cover (1980–2006) from reflectivity time series using SeaWiFS, N7-TOMS, EP-TOMS, SBUV-2, and OMI radiance data

J. R. Herman,[1] G. Labow,[2] N. C. Hsu,[1] and D. Larko[2]

Received 15 October 2007; revised 3 September 2008; accepted 22 September 2008; published 1 January 2009.

[1] The amount of solar radiation reflected back to space or reaching the Earth's surface is primarily governed by the amount of cloud cover and, to a much lesser extent, by Rayleigh scattering, aerosols, and various absorbing gases (e.g., O_3, NO_2, H_2O). A useful measure of the effect of cloud plus aerosol cover is given by the amount that the 331 nm Lambert Equivalent Reflectivity (LER) of a scene exceeds the surface reflectivity for snow/ice-free scenes after Rayleigh scattering has been removed. Twenty-eight years of reflectivity data are available by overlapping data from several satellites: N7 (Nimbus 7, TOMS; 331 nm) from 1979 to 1992, SBUV-2 series (Solar Backscatter Ultraviolet, NOAA; 331 nm) 1985 to 2007, EP (Earth-Probe, TOMS; 331 nm) 1997 to 2006, SW (SeaWiFS; 412 nm) 1998 to 2006, and OMI (Ozone Measuring Instrument; 331 nm) 2004–2007. Only N7 and SW have a sufficiently long data record, Sun-synchronous orbits, and are adequately calibrated for long-term reflectivity trend estimation. Reflectivity data derived from these instruments and the SBUV-2 series are compared during the overlapping years. Key issues in determining long-term reflectivity changes that have occurred during the N7 and SW operating periods are discussed. The largest reflectivity changes in the 412 nm SW LER and 331 nm EP LER are found to occur near the equator and are associated with a large El Nino-Southern Oscillation event. Most other changes that have occurred are regional, such as the apparent cloud decrease over northern Europe since 1998. The fractional occurrence (fraction of days) of high reflectivity values over Hudson Bay, Canada (snow/ice and clouds) appears to have decreased when comparing reflectivity data from 1980 to 1992 to 1997–2006, suggesting shorter duration of ice in Hudson Bay since 1980.

Citation: Herman, J. R., G. Labow, N. C. Hsu, and D. Larko (2009), Changes in cloud and aerosol cover (1980–2006) from reflectivity time series using SeaWiFS, N7-TOMS, EP-TOMS, SBUV-2, and OMI radiance data, *J. Geophys. Res.*, *114*, D01201, doi:10.1029/2007JD009508.

1. Introduction

[2] Daily cloud and aerosol UV reflectivities have been derived from backscattered solar irradiance measurements since 1980 [*Herman et al.*, 2001a, 2001b]. The reflectivities are derived in terms of the Earth's UV Lambert Equivalent Reflectivity (LER; defined in equation (1)), which replaces the physical scene reflectivity with the equivalent reflectivity of a Lambertian surface. The currently available LER data record is from the Total Ozone Mapping Spectrometer (TOMS at 331 nm), the Sea-viewing Wide Field-of-view Sensor (SeaWiFS at 412 nm), the NOAA-SBUV-2 series (Solar Backscatter Ultraviolet at 331 nm), and the Ozone Measuring Instrument (OMI at 331 nm). TOMS is a six-channel cross-track scanning UV spectrometer for measuring ozone, reflectivity, and aerosols with nearly complete global coverage once per day. SBUV-2 is a nadir viewing spectrometer that normally operates with 12 discrete UV channels and gives global coverage once per week. SeaWiFS is an eight-channel cross-track viewing filter spectroradiometer operating mainly in the visible wavelengths from 412 to 885 nm with daily global coverage. OMI is a multifocal plane cross-track viewing spectrometer onboard EOS/AURA measuring from 270 to 500 nm in steps of ~0.5 nm with daily global coverage. The daily LER, combined with Rayleigh scattering, is an important measure of solar radiation reflected back to space as well as providing a means to estimate the fraction reaching the Earth's surface $T(R, R_G)$, where R_G is the reflectivity of the ground and R = LER.

[3] Multiple satellite instruments are included in this study to demonstrate that the variations seen in one data set are present in all of the overlapping data sets and are not instrument artifacts. Because of this, the observed variations can be assigned to changes in cloud and aerosol cover. Model calculations show only small differences between 331 nm and 412 nm reflectivities over clear and cloudy

[1]NASA Goddard Space Flight Center, Greenbelt, Maryland, USA.
[2]Science Systems and Applications, Inc., Lanham, Maryland, USA.

Copyright 2009 by the American Geophysical Union.
0148-0227/09/2007JD009508

scenes, with most of the differences attributable to aerosols. This is especially important when comparing the newly derived SeaWiFS 412 nm reflectivity data with the TOMS and SBUV 331 nm reflectivities. Based on radiative transfer modeling [*Vasilkov et al.*, 2001, 2002, 2005], significant clear-sky differences between 331 nm and 412 nm reflectivities occur over water. For very clean water and water containing colored dissolved organic matter (CDOM), 331 nm is absorbed more strongly than 412 nm, while the reverse is true for water containing only chlorophyll. This modifies the underwater contribution to the measured reflectivity, while the surface Fresnel component of the reflectivity is almost independent of wavelength. The maximum reflectivity observed over ice-free oceans is less than 6 RU at 412 nm and occurs in clean water locations such as the South Pacific Ocean gyre (1 RU = 1% reflectivity, where RU is reflectivity unit).

[4] Since 1980, global warming has gone from an apparently small effect and minor future problem to a major concern. In the future, continued global warming could have dramatic effects on cloud cover as rainfall patterns, land temperatures, and sea surface temperatures change. The changes in downwelling irradiance reaching the Earth's surface associated with changing cloud amounts have long been considered part of a feedback mechanism associated with global warming. Previous studies [e.g., *Somerville and Remer*, 1984; *Tselioudis et al.*, 1992; *Hatzianastassiou et al.*, 2005; *Norris*, 2005] have discussed this problem in detail based on cloud amount data (cloud fraction) determined from visible and infrared wavelengths using the database from International Satellite Cloud Climatology Project (ISCCP) [*Rossow and Schiffer*, 1991] and the Extended Edited Cloud Report Archive (EECRA) [*Hahn and Warren*, 1999] surface observation database. *Norris* [2005] estimates that there was a 1.5% decrease in "sky cover" (cloud cover) over land (1971–1996) and a 1.3% decrease over oceans (1952–1997) based on EECRA data. Good agreement was found between surface-observed EECRA and ISCCP upper-level cloud cover variability during the period of overlap. According to Norris, substantial disagreement occurs between zonal mean time series of surface-observed EECRA and ISCCP low-level and total cloud cover associated with satellite view angle artifacts.

[5] ISCCP can be used as a source of cloud change information (optical depth and cloud fraction derived separately) in addition to the multidecade UV satellite data records listed in Table 1. The ISCCP data are from a combination of geostationary satellites and the polar orbiting Advanced Very High Resolution Radiometer (AVHRR) series where geostationary data are not available. *Evan et al.* [2007] show that the apparent long-term trends in cloud amount (cloud fraction) are caused by limb-darkening and other artifacts from the geostationary portion of the ISCCP data set. A portion of the AVHRR data used in ISCCP were obtained from successive multiple satellites whose orbits slowly drifted in local equator crossing time, so that cloud amounts were sampled at different times of the day in successive years. This causes additional artifacts in the ISCCP cloud time series that are difficult to evaluate, such as the morning to afternoon cloud-amount bias and the bi-directional reflectivity effects of observing clouds at greatly different solar zenith angles. Polar orbiting Sun-synchronous operation minimizes view angle and time-of-day effects with respect to estimating long-term changes within any latitude band and view-angle.

[6] A gridded UV reflectivity data set is ideal for detecting changes in regional and global cloud reflectivity amount, since the low UV surface reflectivity (10 RU > R_G > 2 RU, with most areas less than 4 RU) is nearly constant in time for both land and water in the absence of snow and ice [*Herman and Celarier*, 1997]. Both regional [*Croke et al.*, 1999] and global-scale changes in cloud cover are in response to solar irradiance changes in the atmosphere, and both natural and anthropogenic effects on the Earth [*Bago*, 2002]. In many places, where aerosols containing black carbon are generated in large quantities from industrial activities (e.g., China and India), aerosols directly affect climate, rainfall, and cloud cover [*Surabi Menon et al.*, 2002]. Both short- and long-term changes in cloud cover can change the average surface temperature [*Sun et al.*, 2000]. Detection of changes in the amount of cloud and aerosol cover, which reflects energy back to space, can provide a clear signal of impending regional, and possibly global, climate change.

[7] An example of a single day's UV LER from Earth-Probe-TOMS (EP) is shown in Figure 1, where the white and gray streaks represent the measured reflectivity for R > 10 RU. From the patterns shown in Figure 1, clouds are the major contributors to the reflectivity. Aside from snow and ice, aerosols are the next largest contributor with a reflectivity usually less than 15 RU. In Figure 1, the low UV surface reflectivity features are hidden by an overlaid color map obtained from MODIS visible wavelengths.

[8] The principal modulators of solar UV, visible, and near-IR irradiance (300 to 3000 nm) are cloud transmission, aerosol absorption and scattering, ground reflectivity, and ozone absorption for UVB (280 to 315 nm). At short wavelengths, less than 305 nm, the large ozone absorption coefficient leads to a proportionally large increase in irradiance for a small decrease in ozone (e.g., at 60° solar zenith angle, a 1% decrease in ozone can produce a 4% increase in 305 nm irradiance). Except in cases of dense smoke or dust, aerosols usually reduce radiation reaching the surface by less than 10%. In addition to the above effects, wavelengths in the visible (VIS 400 to 700 nm) are modulated by H_2O and those in the near-IR (NIR 700 to 3000 nm) are modulated by changes in CO_2, CH_4, and H_2O within their respective absorption bands. There is an additional small amount of absorption for UVA and blue wavelengths from NO_2 and from HCHO and for UVB from SO_2, as well as stronger absorption for UV and VIS from smog in urban areas.

[9] Cloud reflectivity/transmission, aerosol effects, and ozone absorption are subject to seasonal and long-term change. To date, most of the long-term ozone change that is large enough to be statistically significant (>1%) has occurred at latitudes greater than 30° in both hemispheres. Long-term regional increases in cloud plus aerosol reflectivity will cause corresponding decreases in UVB irradiance that can be larger in magnitude than those caused by the observed ozone changes, especially at lower latitudes. Clouds and aerosols similarly affect all other solar wavelengths reaching the Earth's surface between 280 and 3000 nm. Outside of the UV wavelengths, seasonally

Table 1. Currently Available UV or Near-UV Reflectivity Data Sets

Years	Data Set	Description
1979–1992	Nimbus-7/TOMS (N7)	The 331 nm daily reflectivity is produced as part of standard processing using in-flight calibration. Full global coverage every day. Only a few missing days from1980 to 1992.
1985–2008	SBUV-2 Series (N-9, N-11, N-16, N-17, N-18)	The 331 nm daily reflectivity is produced as part of standard processing using in-flight calibration. There are 14 nadir-viewing orbits per day. Full global coverage once per week. Only a few missing days. Additional data are available from N-17 (2002) and N-18 (2005). Unlike N-16 (2000), N-17, and N-18, N-9 (1984), and N-11 (1998) have to be used with caution, since they have drifting orbits (changing equator crossing times).
1996–2006	Earth-Probe/TOMS (EP)	The new recalibrated 331 nm daily reflectivity is produced as part of standard processing. Full global coverage every day. Only a few missing days in 10 years. The calibration precision was improved by using N-16 as a reference but does not have the precision for trend computation.
1997–2008	SeaWiFS (SW)	The 412 nm reflectivity has been produced using the TOMS production algorithm and in-flight SeaWiFS calibration. The precision is very high. However, high latitude data (>60°) is limited to summer months. The plane of cross-track scanning is tilted 20° away from the sun to avoid ocean sun glint.
2004–2008	Ozone Monitoring Instrument (OMI)	The 331 nm daily reflectivity is produced as part of standard OMI processing using in-flight calibration. Full global coverage every day. Reflectivity values are available for all wavelengths from 330 nm to 500 nm. However, different detectors and calibrations in multiple focal planes currently make it difficult to relate 412 nm visible to 331 nm UV wavelengths with high precision.

varying land-surface reflectivity is an important component of the total scene reflectivity. Ice-free diffuse ocean reflectivity is low (<10 RU) [*Morel and Prieur*, 1977] for all visible wavelengths during all seasons and becomes less than 1 RU for wavelengths longer than 700 nm. Specular Fresnel reflectivity (ocean glint) from the oceans can be quite large at all wavelengths. Glint is seen by TOMS and SBUV-2 only in narrow geographic bands at low latitudes but is not present in SW data because of instrument design.

[10] The reflectivity associated with aerosols is a function of wavelength that varies with the particle size and type of aerosol (e.g., dust, smoke, or industrial aerosol). Cloud reflectivity is almost independent of wavelength in the UV-visible part of the spectrum because of its large average particle size relative to the wavelength of light. For wavelengths longer than 3 microns, the effective outgoing radiation from the Earth starts to include significant thermal components from the atmosphere and surface.

[11] Table 1 lists the available UV and 412 nm data suitable for estimating changes in cloud reflectivity. Previous studies have described reflectivity changes using TOMS measurements of UV radiance changes within the period 1980 to 1992 [*Herman et al.*, 1996, 2001a, 2001b; *Eck et al.*, 1987, 1995], and using ERBE infrared cloud optical depths [*Lubin et al.*, 1998]. The latter are difficult to relate to cloud reflectivity or cloud amount. The data gap from 1993 to mid-1996 in the Total Ozone Mapping Spectrometer (TOMS) series complicates the application of reflectivity records to determine long-term global and regional changes in cloud, aerosol, and surface UV amounts. In the future, the long-term 331 nm reflectivity data from the NOAA SBUV-2 series of satellites (1985 to 2007) can fill

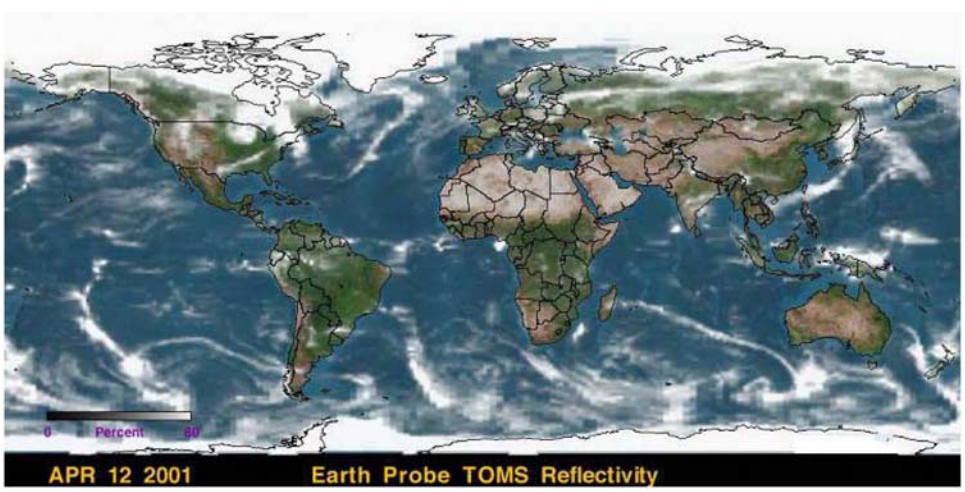

Figure 1. UV reflectivity derived from TOMS measured radiances. The background color map is from MODIS visible wavelengths with the green areas representing vegetation. In the UV, the background would be dark with reflectivity from 4 to 10 RU (1 RU = 1% reflectivity).

in the gap after a careful recalibration of SBUV-2 measured radiances. The 331 nm UV data record can be extended using OMI estimated LER values for 2004 to 2008, and for the OMI satellite lifetime.

[12] This study will focus on the effects of changes in cloud cover and aerosol amounts as represented by the LER for UV and visible irradiance at the Earth's surface based on the measured radiances from SeaWiFS (412 nm, 1998 to 2006). The new results are compared with the reflectivity changes that were observed in the Version-8 reflectivity time series from Nimbus7-TOMS, the new (2007) recalibrated EP-TOMS, OMI, and the NOAA-SBUV-2 series of instruments (see Table 1). The reflectivity over Hudson Bay is used to estimate the long-term precision of both SeaWiFS and Nimbus-7/TOMS and to detect a possible change in reflectivity that may be associated with global warming.

[13] After defining the Lambert Equivalent Reflectivity, the similar zonal average reflectivities are shown for five different satellite instruments. We discuss some problems associated with long-term trend estimations from ground-based cloud observations. Section 2 discusses the calibration of TOMS, SeaWiFS, and OMI. Section 3 shows an example of the general long-term behavior of the reflectivity from combining all of the available UV reflectivity data and shows the correlation between pairs of reflectivity time series from different satellites. Section 4 shows details from the zonal average time series, section 5 discusses the long-term zonal average trends, and section 6 discusses the long-term reflectivity trends as a function of latitude and longitude. For estimation of long-term reflectivity changes, this paper will consider only N7-TOMS and SeaWiFS, since their radiance data were obtained near local noon, and they have well-maintained in-flight calibrations.

1.1. Lambert Equivalent Reflectivity

[14] The Lambert Equivalent Reflectivity R represents the equivalent scene reflectivity (the combined effect of the surface R_G, clouds, water haze, and aerosols) after removal of Rayleigh scattering effects. For the satellite data presented here, R is an approximation to the angular average reflectivity, since it is based on only a small subset of the Earth's BRDF (bidirectional reflectivity distribution function) from views between ±53° in a direction approximately perpendicular to the orbital plane.

[15] R is calculated by requiring that the measured radiance I_{SM} match the calculated radiance I_S at the observing position of the satellite (equation (1)) by adjusting a single free parameter R in the formal solution of the radiative transfer equation

$$I_S(\Omega,\Theta,R,P_O) = \frac{RI_d(\Omega,\Theta,P_O)f(\Omega,\Theta,P_O)}{1-RS_b(\Omega,P_O)} + I_{dO}(\Omega,\Theta,P_O) = I_{SM} \tag{1}$$

where Ω is the ozone amount from shorter wavelengths (e.g., 317 nm), Θ is the viewing geometry (solar zenith angle, satellite look angle, azimuth angle), R is LER at P_O, P_O is pressure of the reflecting surface assumed at the local ground altitude. S_b is fraction scattered back to P_O from the atmosphere, I_d is the sum of direct and diffuse irradiance reaching P_O, f is the fraction of radiation reflected from P_O reaching the satellite, and I_{dO} is the radiance scattered back from the atmosphere for R = 0 and P = P_O.

[16] From equation (1),

$$R = \frac{I_{SM} - I_{dO}}{I_d f + (I_{SM} - I_{dO})S_b} \tag{2}$$

The values of R for wavelengths greater than 340 nm can be calculated directly from equation (2). Estimating R for wavelengths shorter than 340 nm requires knowing the ozone amount. For all wavelengths, we require accurate specification of the background multiple-scattering molecular atmosphere.

[17] Measurements of UV reflectivity over a moderately large scene (e.g., of dimension 10 to 100 km) containing a number of clouds is a good approximation to the combined affects of cloud optical depth and cloud fraction on reflected and transmitted radiation without needing a detailed cloud model. This is especially important where the clouds are complex mixtures of oddly shaped structures, with self-shadowing and multiple layers, where no accurate model exists to convert cloud physical properties into cloud transmission under all conditions.

[18] The measured UV reflectivity R can be approximately converted into the transmission T of radiation to the Earth's surface, $C_T \approx T = (1 - R)/(1 - R_G)$, for solar ultraviolet (UV = 280–400 nm) and visible (VIS = 400–700 nm) irradiance reaching the Earth's troposphere and surface through a cloud layer (see Appendix A and *Krotkov et al.* [2001]). More accurate estimations have been developed [*Krotkov et al.*, 2001] for cloud transmission C_T using radiative transfer calculations for clouds over a UV ground reflectivity R_G [*Herman and Celarier*, 1997]. The more accurate estimations of C_T are approximately equal to T for analyzed scenes from TOMS data.

[19] The assumption of Lambert Equivalent Reflectivity to represent the actual non-Lambertian BRDF will lead to an error in the estimation of the total radiation reflected back to space each day, but not in the year-to-year percent change. Since the TOMS and SeaWiFS reflectivity data are obtained from satellites in near-noon Sun synchronous orbits, the viewing geometries are approximately equivalent for the same day of each year. We assume that the year-to-year change in LER at a given location (repeatable viewing angles and SZA for the same day of each year) can be used to accurately estimate the corresponding long-term changes in reflected radiation from clouds and aerosols.

[20] The easiest way to compare the various available reflectivity time series is by forming a zonal average for each 5° latitude band, averaged over each satellite's multi-year record (see Table 1). Figure 2 shows a comparison of the zonal average reflectivities (ZARs) produced by five independent satellite instruments that are close in magnitude and show similar features. They should not agree exactly, since they represent different periods, and in the case of SeaWiFS, a different wavelength. The ZAR for N7-TOMS is different in the equatorial region near 5°N because of a weaker El Nino-Southern Oscillation (ENSO) effect during the years 1980 to 1992 compared to 1997 to 2007. As will be discussed later, there are also regional long-term increases and decreases in reflectivity in both the Northern and Southern Hemispheres, especially the cloud decreases

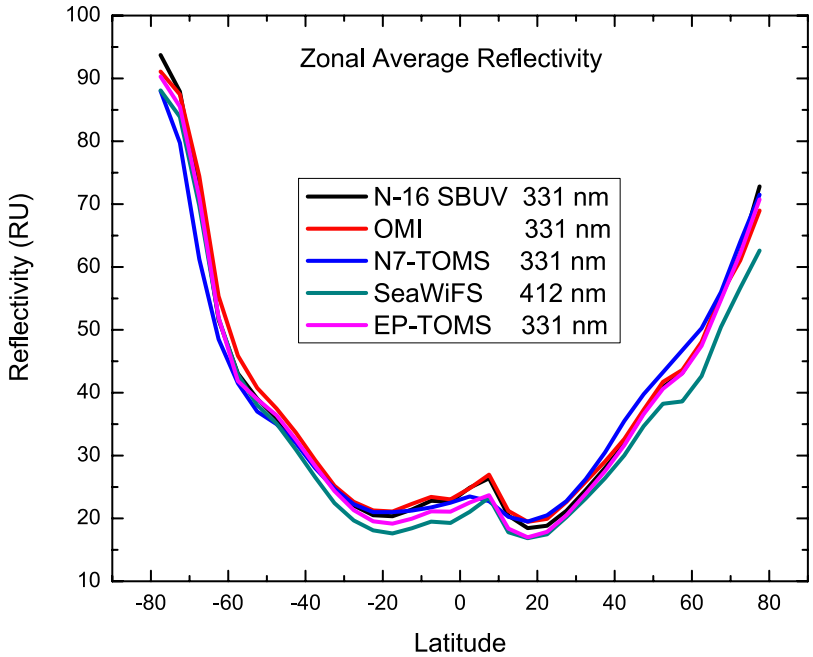

Figure 2. The zonal average reflectivity data sets from SBUV-2 (331 nm), OMI (331 nm), EP-TOMS (331 nm), N7-TOMS (331 nm), and SeaWiFS (412 nm) for their various years of operation.

(UV increases) seen in Australia, which already has a major skin cancer problem caused by unusually high UV exposure compared to similar latitudes in the Northern Hemisphere with fewer cloud-free days.

1.2. Ground-Based Observations

[21] Detecting long-term area-average cloud transmission changes from well-calibrated ground-based irradiance observations is not presently possible because of the large meteorological variance at any particular location. From the viewpoint of satellite observations, major seasonal cloud patterns repeat with approximate regularity from year to year. This permits much of the interannual variance to be removed through regional or zonal averages. For fixed location ground-based observations, the major seasonal cloud patterns shift slightly with respect to latitude and longitude, giving rise to an apparent large observed interannual radiance and irradiance variance that is difficult to remove from the data. Additional irradiance variances arise for both satellite and ground-based observations driven by quasiperiodic occurrences such as the El Nino-Southern Oscillation (ENSO) events originating in the equatorial Pacific Ocean, solar cycle changes, and the Quasi-Biennial Oscillation (QBO). These events directly affect UV irradiance amounts and trend estimates based on deriving UV time series coefficients for terms with proxy variation, such as the 10.7 cm solar flux representing the ~11-year solar cycle and the Singapore winds representing the ~2.3-year QBO. The nearly regular solar cycle and QBO effects can be modeled and removed from the reflectivity time series before trend estimation. The irregular ENSO effect on trend estimation can be significant for moderate-term data records available from most satellite and ground-based observations. High precision UV satellite data records have been available since 1979 (currently 28 years), during which there have only been a few major ENSO events of varying magnitude and duration. Because of the irregularity, the ENSO effects cannot be removed from the trend calculations for global reflectance or UV irradiance in a manner similar to that used for the QBO effect [*Stolarski et al.* 1991; *Herman et al.*, 1991a, 1991b, 2000].

2. Calibration of N7-TOMS, EP-TOMS, SeaWiFS, and OMI

[22] The calibration problems associated with the TOMS and SBUV-2 measurements of ozone amounts have been sufficiently overcome to permit the estimation of long-term ozone trends [e.g., *Stolarski et al.* 1991; *Hollandsworth et al.*, 1995; *McPeters et al.*, 1996]. The retrieval of ozone amount is from the measured ratio of radiances at two or more wavelengths with only a small contribution from the scene reflectivity. The formation of the radiance ratios cancels out most of the instrument calibration errors. However, reflectivity is inherently a single-wavelength measurement, so that both absolute radiometric calibration (accuracy) and relative time-dependent calibration (precision) are required for daily estimations of irradiance at the Earth's surface. Observations of particularly stable regions of the Earth can help establish precision and adequately verify both accuracy and precision of single-satellite scene reflectivity estimates [*Herman et al.*, 1999].

2.1. Hudson Bay

[23] A useful location for a comparison of TOMS, SW, and OMI reflectivity time series is for data obtained in a 1° × 1° box over Hudson Bay, Canada at 54.5°N, 80.5°W. The SBUV-2 series has too large a field of view (200 km) to use this southern portion of Hudson Bay, but can use a wider portion of the bay that is further north. In the

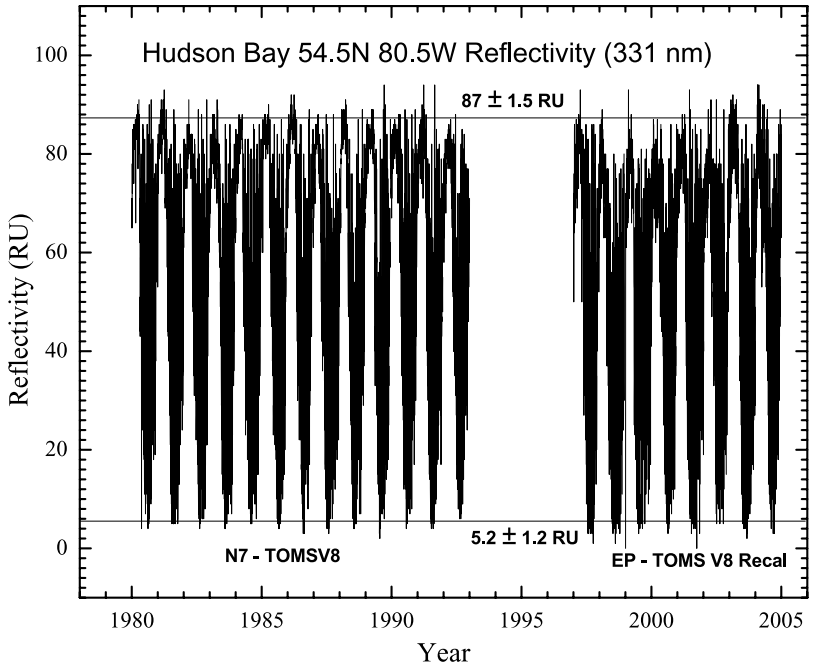

Figure 3. N7-TOMS, 1980 to 1993, and EP-TOMS, 1998 to 2004, 331 nm reflectivity over Hudson Bay Canada from Version 8 data on the TOMS website with EP recalibrated referenced to N-16.

Hudson Bay there is open water during the summer (low UV reflectivity ~5 ± 1 RU) and snow over ice during the winter (high UV reflectivity ~87 ± 1.5 RU). The ice at Hudson Bay is newly formed each year and covered with recent snow forming a relatively flat surface (limited shadows) whose reflectivity is fairly constant from year to year. As expected, the reflectivity reaches a maximum for clear days during January–February and a minimum for clear days during June–July.

2.2. TOMS

[24] If the in-flight instrument calibration is effective, these maximum and minimum reflectivity values should appear each year with only a small variance as has been shown for N7-TOMS [*Herman et al.*, 2001b] 380 nm reflectivity. Figure 3 shows similar results for 331 nm reflectivity both N7 (87 ± 1.6, 5.2 ± 1.2 RU) using the recent Version 8 TOMS data and EP (86.9 ± 1.6, 5.3 ± 1.5 RU), with the new EP data normalized to N-16 to partially remove a calibration error.

[25] Here, the agreement between N7 and EP is within 1 RU. For a satellite instrument, this still leaves the question of whether the long-term calibration is constant with respect to latitude. For example, Earth-Probe TOMS has an ascending orbit (south to north on the daylight side) and underwent frequent solar calibrations as it emerged into sunlight over Antarctica. The combination of solar calibration over Antarctica and the constancy of the reflectivity observations over Hudson Bay, Canada (~53°N) should have ensured that Earth-Probe TOMS data had long-term radiometric precision as a function of latitude. For EP/TOMS, the absolute calibration is based on a combination of preflight laboratory and in-flight calibration by viewing the sun using a system of three diffuser plates, with one rarely exposed so as to maintain a long-term reference. EP's better preflight and in-flight calibration, compared to Nimbus-7 TOMS (one diffuser plate), should have been satisfactory, but the results for long-term EP-TOMS radiometric precision have been disappointing. The solar and surface calibrations were not sufficient for Earth-Probe TOMS, which showed abnormally large increases in high-latitude (>40°S) Southern Hemisphere reflectivities, especially after 2003. EP-TOMS gradually developed an apparent problem with its scan mirror, so that instrument throughput changes as a function of latitude, scan position, and a function of wavelength either through erosion or a coating of the scan mirror. If this hypothesis of the EP instrument problem is correct, then the solar calibration viewing the sun striking a diffuser plate at a fixed scan-mirror angle was not representative of the Earth observations. This problem significantly affected both the estimation of reflectivity and the aerosol index after 2002 and was evident earlier in the data record. A recent renormalization of EP measured radiances, using NOAA-SBUV2/16 (N-16) as a reference, has improved the precision of the calculated LER values over a longer period as is shown later. Because of remaining scan mirror problems, especially in the Southern Hemisphere, the EP reflectivity data are still not used for estimation of trends.

[26] For the N7/TOMS instrument, the absolute and relative wavelength-to-wavelength accuracy were maintained by in-flight calibration using corrections to a slowly degrading Sun-viewing onboard diffuser plate [*Herman et al.*, 1991a, 1991b]. The successfully achieved goal was to maintain relative and absolute radiance calibration capable of producing ozone value, precise to within 1% over a decade, which is needed to determine ozone trends [*Stolarski et al.*, 1991; *Herman et al.*, 1991a, 1991b]. This meant successfully

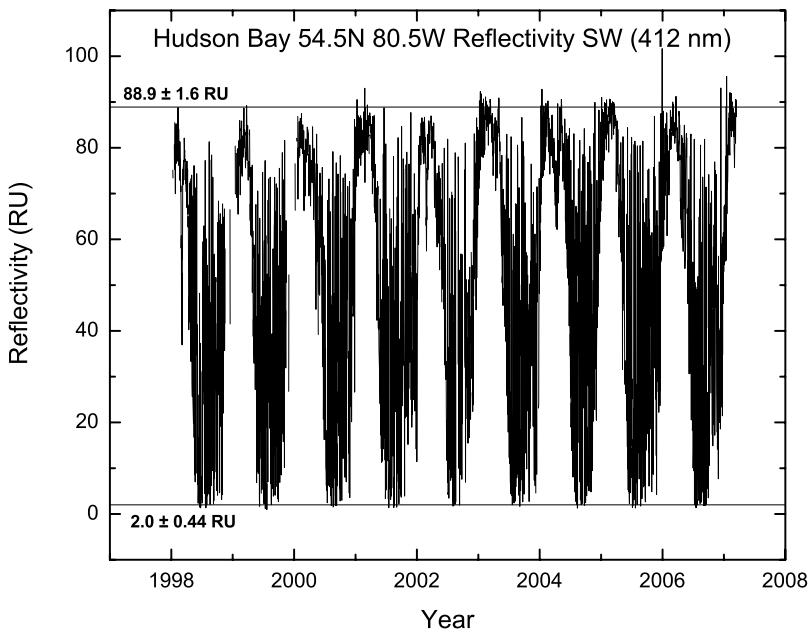

Figure 4. SeaWiFS Hudson Bay 412 nm reflectivity for 1998 to 2007.

obtaining the single channel radiances used for reflectivity to within 3% precision.

[27] For reflectivity, the best that can be expected is a precision of about 3% per decade based on equation (2). This translates into a precision of 3 RU/decade for very high reflectivity scenes and 0.5 RU/decade for typical low reflectivity scenes. On the basis of the Hudson Bay results, good precision was achieved for N7, EP, and SW (Figures 3 and 4) over the indicated periods. The estimates for the upper bound line 87 ± 1.5 RU and lower bound line 5.2 ± 1.2 RU in Figure 3 are determined from the averages and standard deviations of time series from the annual maxima and minima after removing two outlier points from each year (similarly for SW in Figure 4). The estimated precision includes both instrumental and geophysical variability.

2.3. SeaWiFS

[28] The visible radiance measurements (1998 to present) from SW are also calibrated in-flight using a combination of lunar, solar, and ocean-based vicarious calibration observations [*Eplee et al.*, 2001]. The result has been a stable radiance data set of precision comparable to those from Nimbus-7 TOMS. The equivalent Hudson Bay reflectivities for SW (88.9 ± 1.6, 2 ± 0.44 RU) are different than TOMS during the low-reflectivity summer months. Aside from calibration, there are two significant differences: (1) SW observes at 412 nm and (2) the observations are made in a plane tilted 20° from nadir (center pixel) in the anti-Sun direction, while TOMS observes in a plane passing through nadir.

[29] Forming histograms of N7 and SW reflectivities in 1 RU bins (Figure 5) shows that the most frequently occurring reflectivity, 83 RU, occurs 3.4% of the time for N7 and 2.8% for SW. Such high reflectivities are due to ice plus snow in fairly cloud-free scenes. With a similar histogram for EP, there is a shift in histogram maximum (76 RU) relative to SW (83 RU) and N7 (83 RU), which suggests that EP is still not properly calibrated with sufficient accuracy to be used for reflectivity change studies. The higher reflectivities occur for scenes containing snow over ice, with and without clouds, so that the most frequently occurring reflectivity values for Hudson Bay should not substantially change with time up to the end of 2006. SW is showing a significant decrease in fractional occurrence of reflectivities between 80 and 90 RU and an increase in reflectivities less than 60 RU. The shift in fractional occurrence may be an indicator of a change toward shorter winters with less duration of ice. This is in agreement with observations of reduction in seasonal ice duration in the southwestern Hudson Bay from 1971 to 2003 [*Cornwell et al.*, 2004].

[30] Compared to TOMS, the biggest SW difference is that the geographic coverage of the Polar Regions was limited to observing conditions when the solar zenith angle is less than 65°. During the winter solstice, coverage is limited to latitudes less than 47°, while during the summer solstice, SeaWiFS coverage extends to the poles. For example, there are winter sampling problems for the southern tip of South America (55°S), Northern Canada, the Arctic, and Antarctica. For this reason SeaWiFS annual trend estimates should be limited to about the ±50° latitude range.

[31] At the lowest summer values, EP has a reflectivity value of about 5.3 ± 1.2 RU (Figure 3), while SW is about 2 ± 0.44 RU (Figure 4). The difference is not likely to be from water leaving radiances, since water absorbs more at 331 nm than at 412. The predominant absorbing material in Hudson Bay during the summer is dissolved organic matter (DOM), which absorbs more at 331 nm than at 412 nm. The larger component, from Fresnel surface reflection, is almost independent of wavelength.

[32] The SeaWiFS radiance data used in this paper were archived at 4 × 4 km^2 pixels. These were summed to obtain the TOMS equivalent pixel radiance (mW/(m^2 nm sr)) at the

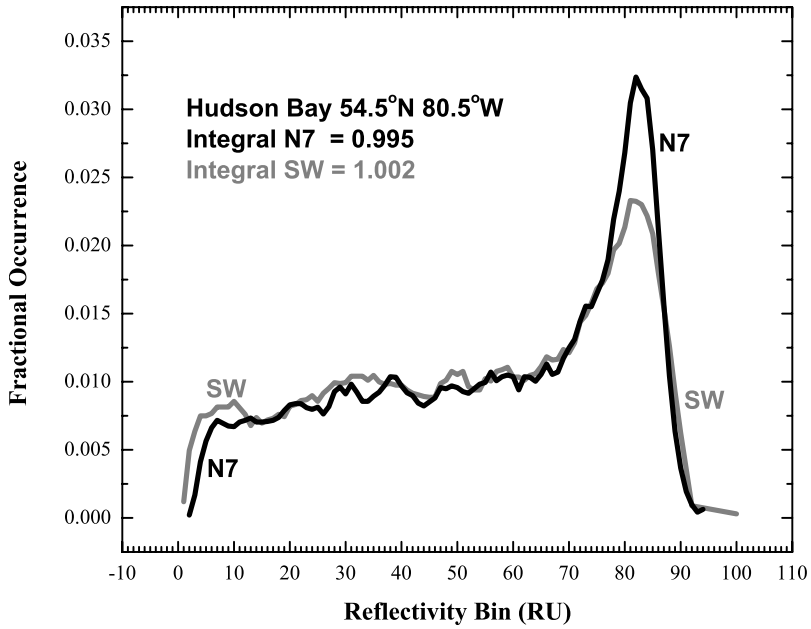

Figure 5. Histogram of fraction of occurrence for reflectivity bins from 0 to 100 RU in steps of 1 RU for N7 and SW. The integrals for each histogram should equal 1.

top of the atmosphere with a spatial resolution of 1° × 1°. The SW spatially equivalent 412 nm radiances were then converted into scene reflectivity using the TOMS LER standard algorithm based on equation (2). The SW radiometric calibration has been maintained to high precision using solar, lunar, and in situ ''vicarious'' calibration techniques [*Barnes and Holmes*, 1993; *Barnes et al.*, 1996; *Eplee et al.*, 2001]. Possible cross-track scan errors are held to a minimum by using a rotating telescope design to eliminate polarization effects that can occur when using an external scan mirror. The plane of the rotating telescope is tilted at 20° from nadir away from the sun to avoid sea-glint contamination. The longest wavelength for EP/TOMS is 360 nm, while the shortest SeaWiFS wavelength is 412 nm, so that there is no direct overlap in either view angle or wavelength for the two satellites. Since the scene reflectivity for land and water is quite low at both wavelengths, less than 10 RU, clouds, aerosols, and snow/ice dominate both long- and short-term changes in the scene reflectivity.

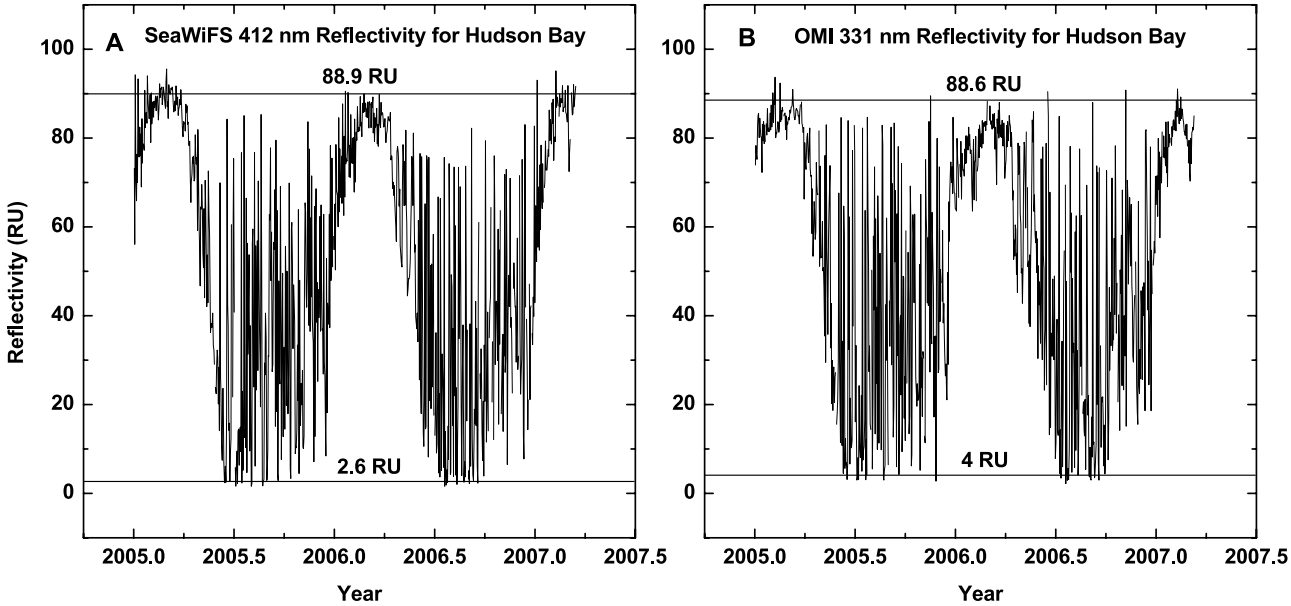

Figure 6. (a) SeaWiFS 412 nm reflectivity over Hudson Bay, Canada, from 2005 to 2007. (b) OMI 331 nm reflectivity over Hudson Bay, Canada, from 2005 to 2007.

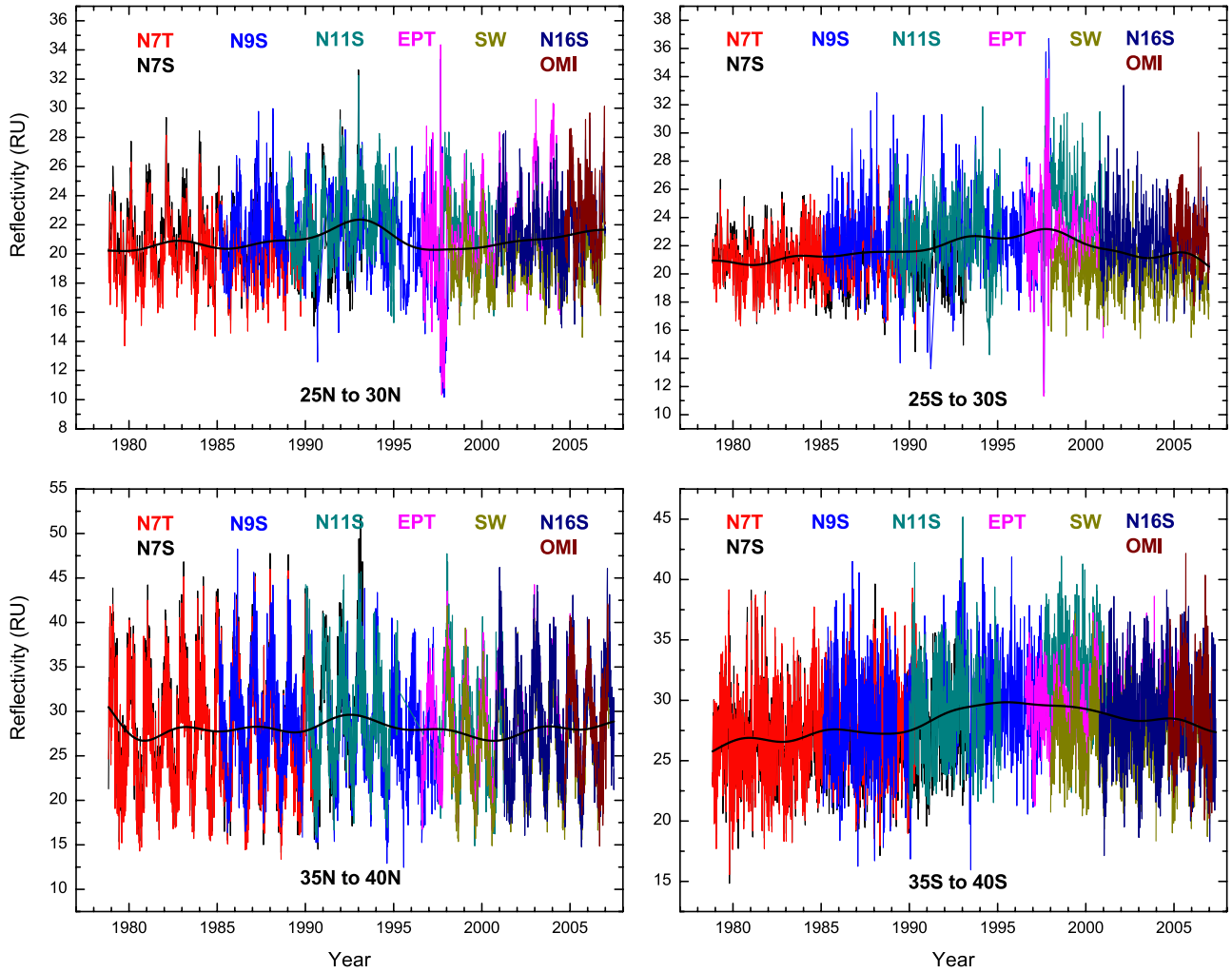

Figure 7. Reflectivity time series constructed from Nimbus7-TOMS, Nimbus7-SBUV, NOAA-SBUV-9, NOAA-SBUV-11, NOAA-SBUV-16, Earth-Probe-TOMS, SeaWiFS, and OMI for two sample 5°-wide latitude bands centered at 25°N–30°N, 25°S–30°S, 35°N–40°N, and 35°S–40°S. The smooth black line is a 24-month FFT low-pass filter of all data sets showing the general average behavior of reflectivity versus time.

2.4. OMI

[33] An additional cross-instrument check of SW stability can be obtained from a comparison with the recently launched (2004) OMI spectrometer (Figures 6a and 6b) for the period from 2005 to 2007. The average maxima are almost the same (88.9 versus 88.6 RU), but the minima differ by about 1.4 RU, with the year-to-year variability almost the same. The OMI minima are in agreement with TOMS.

[34] While there are differences in the absolute reflectivities from all satellite data sets over Hudson Bay, both the minimum and maximum annual reflectivities are nearly constant, and show no trend, suggesting that the in-flight calibrations were successful in producing a radiance data set with annual repeatability for conditions of clear-sky over snow/ice or clear-sky over water. The long-term constancy of the SW Hudson Bay reflectivity indicates that the in-flight calibration has sufficient precision for the computation of multiyear trends in reflectivity at other locations. For this purpose, we will use the 9-year SW reflectivity data set (1998–2006), since it has the longest current data record, and is still obtaining new data, having no problems with Earth observations, or with in-flight calibration.

3. Combined Data

[35] Ultimately, it is desirable to combine the multiple-satellite reflectivity data sets from 1979 to the present to create a continuous record of long-term changes in cloud and aerosol cover. Because of differences in calibration, the various time series cannot be simply joined, but will have to be reprocessed with new in-flight calibration coefficients. A preliminary example of an uncorrected combined data set is shown in Figure 7 for four 5° wide latitude bands centered on 27.5°N, 37.5°N, 27.5°S, and 37.5°S, where NOAA SBUV-2 data (N-9, N-11, and N-16) are used to fill in the gaps and are combined with N7, EP, and SW. Of interest is the overall average behavior shown in Figure 6 by a 24-month Fourier Transform (FFT) low-pass filter applied to the average of all the data sets. Similar, but

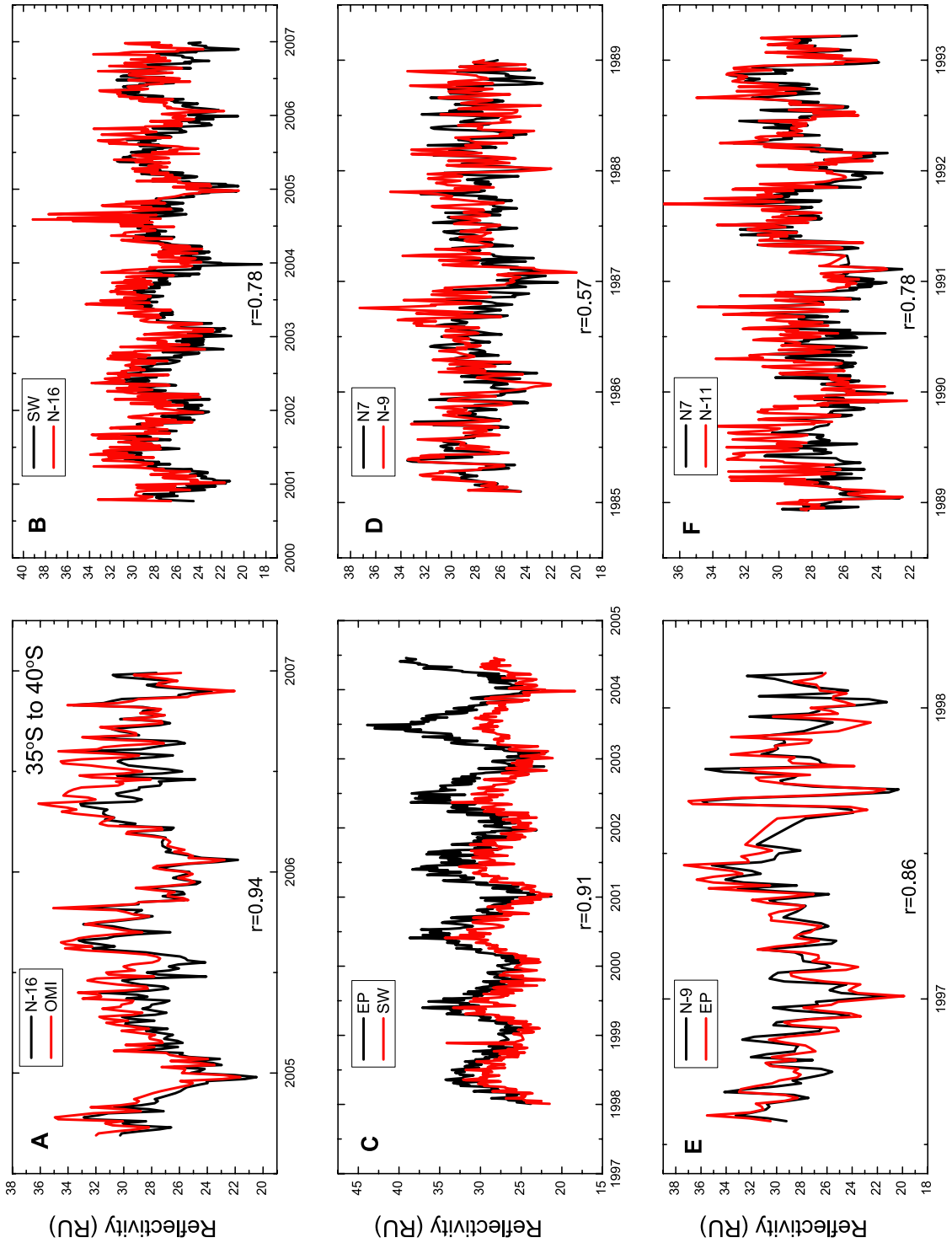

Figure 8. Correlation between different satellite measurements of 5-day averaged reflectivity in the bands 35°S–40°S and 35°N–40°N. (a) N-16, OMI, (b) SW, N-16, (c) EP, SW, (d) N7, N-9, (e) N-9,EP, (f) N7, N-11, (g) N-16, OMI, (h) SW, N-16, (i) EP, SW, (j) N7, N-9, (k) N-9,EP, (l) N7, N-11.

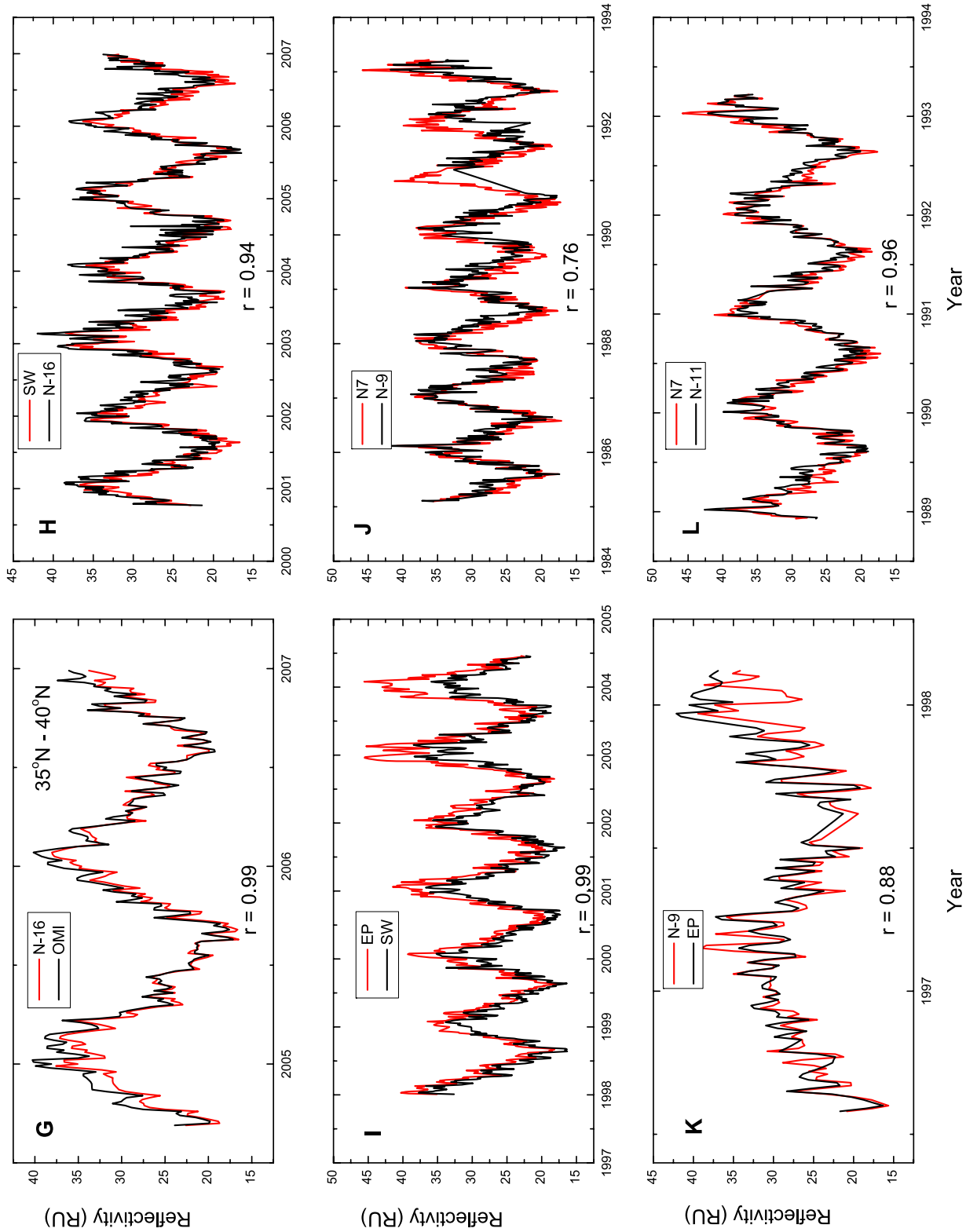

Figure 8. (continued)

noisier, results are obtained using adjacent averaging in place of the FFT low-pass filter.

[36] The seasonal behavior of the multisatellite 27.5°N and 37.5°N reflectivity time series differs from that in the Southern Hemisphere because of the different ratio of land to ocean. At northern midlatitudes, there is a much larger contribution of winter snow and ice to the reflectivity than at southern midlatitudes. Also visible is a peak in 1992–1993 at 27.5°N and in 1997–1998 at 27.5°S. There is a minimum at 27.5°N in 1997 to 1998 that corresponds to the maximum at 27.5°S. The sharp maximum and minimum are in the reflectivity data sets from both EP-TOMS and SeaWiFS. The 1997–1998 reflectivity maximum and minimum are correlated with a strong El Nino event in the central Pacific Ocean. The El Nino effect is diminished at 37.5°N and not apparent at 37.5°S. The El-Nino event is associated with an increase in sea surface temperature (SST) as measured by the NOAA Tropical Atmosphere Ocean Project (TAO), which consists of approximately 70 moorings in the Tropical Pacific Ocean [*Smith*, 1995].

[37] At 27.5°N there has been long-term upward drift of about 2 RU between 1998 and 2006, and a decrease of about 3 RU at 27.5°S. Applying a simple linear fit after 1998 gives an estimated increase in zonal average reflectivity at 27.5°N of 0.16 ± 0.06 RU/year and a decrease at 27.5°S of 0.2 ± 0.03 RU/year. SeaWiFS by itself shows an increase of 0.11 ± 0.07 RU/year at 27.5°N and a decrease of 0.1 ± 0.04 RU/year at 27.5°S, only a little different than the combined time series. Similar changes are seen at 37.5°S and 37.5°N. These results may change slightly when a thorough recalibration is performed for all of the contributing satellite instruments to obtain a consistent time series for the entire period, 1979–2007.

[38] Even without the recalibration, there are detailed correlations of seasonal and inter-seasonal features between the various time series from different satellites, although the absolute calibrations are not yet sufficiently compatible (Figures 7 and 8). For example, in Figure 7, both EP and N-9 match at 27.5°, even for an extreme low value seen on 27 October 1997 (RU = 13.0 and 13.8 RU, respectively), and are highly correlated (0.86).

[39] Figure 8 shows the correlations and correlation coefficients between six overlapping pairs of uncorrected reflectivity data sets for the latitude bands 35°S–40°S and 35°N–40°N. The purpose of Figure 8 is to show that the observed features, even the small details, are not instrument artifacts, but are observed by multiple independent instruments. Figures 8a and 8g show that OMI and N-16 agree within 2 RU and are highly correlated ($r > 0.9$). Figures 8b and 8h compare SW and N-16 showing a 2 RU offset in Figure 8b and ($r = 0.78$) and no offset in Figure 8h ($r > 0.9$). Figures 8c and 8i compare SW and EP showing a rapidly separating calibration drift caused by EP, but with high correlation ($r > 0.9$). Figures 8d and 8j show that there are only small calibration differences between N-9 and N7, but the daily values differ because of the drifting N-9 orbit, giving rise to a lower correlation for the 1985 to 1989 overlap.

[40] Figures 8e and 8k compare EP with N-9 during the first 2 years of EP, showing good calibration agreement and high correlation ($r > 0.85$). Figures 8f and 8l show that there is good calibration agreement between N-11 compared to N7 for the 1989 to 1993 overlap and have moderate correlation in Figure 8f ($r = 0.78$) and good correlation in Figure 8l ($r > 0.9$) even though the broader features match well. Multi-instrument comparisons at other latitude bands are different than those for the ±27.5° and ±37.5° bands, suggesting that there will be considerable difficulty in creating a joined reflectivity time series as a function of latitude between ±65° with a common calibration. The combination of different fields of view, daily coverage, and for N-9 and N-11, drifting orbits, will complicate the problem.

4. Zonal Average Reflectivity Time Series

[41] Using a global grid of reflectivities, the annual and zonal average latitude dependence of the reflectivity can be obtained for N7 (1980–1992) and EP (1998–2004), OMI (2004–2007), and SW (1998–2006) and plotted as pairs for comparison (Figure 9). From Figure 9a, it is clear the EP and SW zonal average reflectivities agree fairly well, except at northern latitudes above 50°. OMI and SW (Figure 9b) are displaced slightly from each other indicating a difference in calibration or a difference caused by the shorter OMI time series (2004–2006). However, OMI and EP agree quite closely as shown in Figure 9e. The comparisons shown in Figures 6–8 show that the detailed features of each reflectivity time series are not from instrument artifacts but represent physical changes in the observed scenes. However, differences in calibration (e.g., those shown in Figures 7 and 8) currently prevent the use these time series for an estimate of reflectivity change over the entire period from 1979 to 2007. Accordingly, the remainder of the paper will focus on trends derived from SeaWiFS and Nimbus-7/TOMS.

[42] The SW zonal average time series for each 5° latitude band between −55° and 55° are shown in Figure 10 for the years 1998 to 2006. Figure 10 is similar to one for Nimbus-7/TOMS [*Herman et al.*, 2001b] but with 5° bands instead of 10°. The equatorial zone in the range ±5° shows almost no seasonal cycle. Between 5° and 15° in both hemispheres the reflectivity has a maximum during summer caused by the motions of the Intertropical Convergence Zone (ITCZ) band of clouds, located north of the equator during April to August and south of the equator during October to February. At higher latitudes, greater than 25°N and 30°S, the reflectivity has a maximum in the winter, January and June, respectively, caused by the presence of snow and by the lack of high reflectivity tropical clouds. There is a transition zone between these two regimes from 20°N to 25°N and from 20°S to 30°S, where there is almost no seasonal dependence in zonal average cloud cover. In the Southern Hemisphere, the seasonal dependence almost disappears for latitudes between 45°S and 55°S because of the small amount of land area compared to ocean. This is in contrast to the Northern Hemisphere where land and snow cover dominate at high latitudes. The large increase in equatorial reflectivity in the beginning of 1998 corresponds to a large ENSO event that

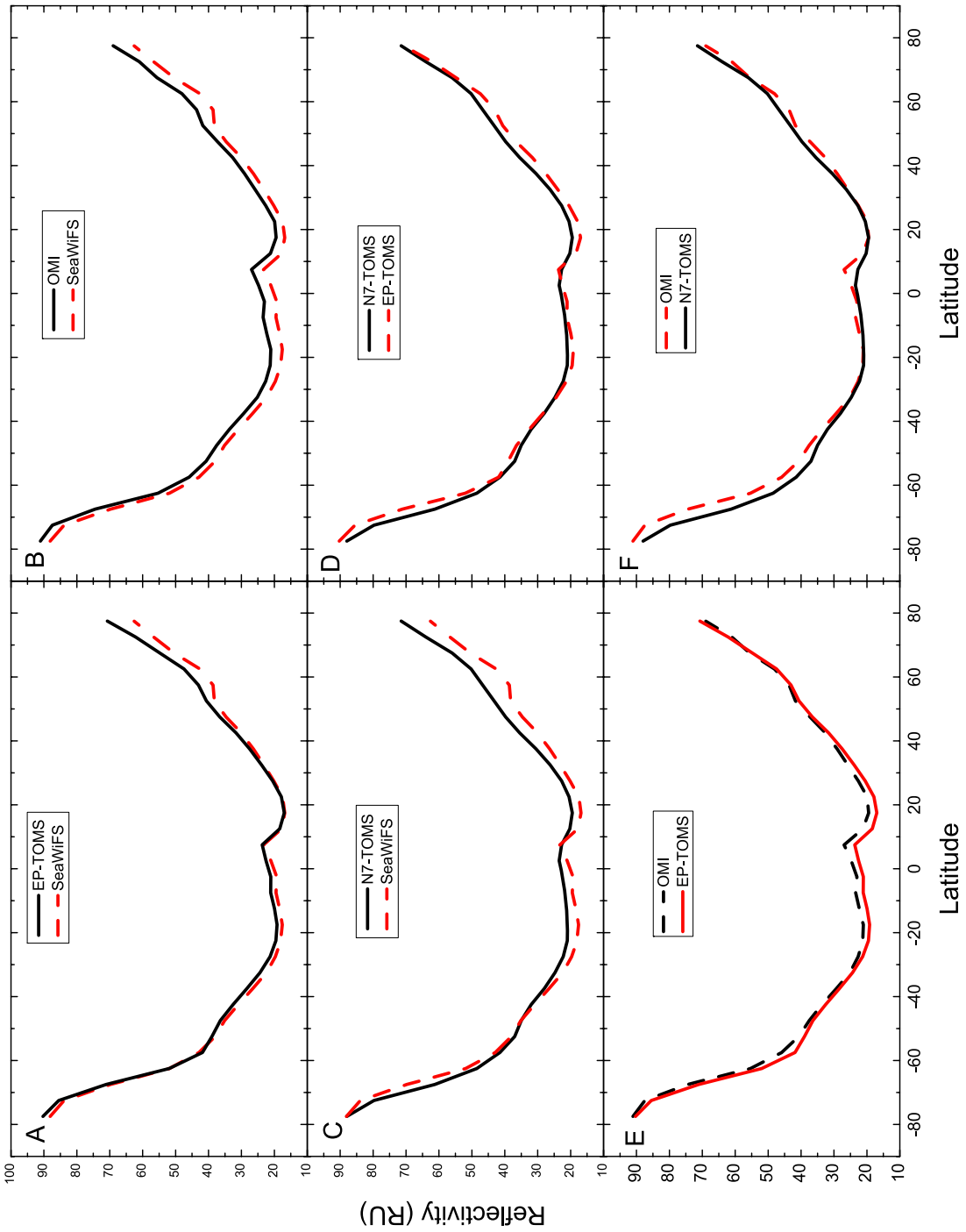

Figure 9. The zonal average reflectivity data sets from OMI (331 nm), EP-TOMS (331 nm), N7-TOMS (331 nm), and SeaWiFS (SW) (412 nm) for various years of operation. (a, b, and c) Comparisons with SW as a reference; (d) a comparison between the N7 and EP TOMS instruments; and (e and f) comparisons with OMI as a reference. Figure 9b also has OMI as a reference. Of these, only SW and EP cover the same period (Figure 9a).

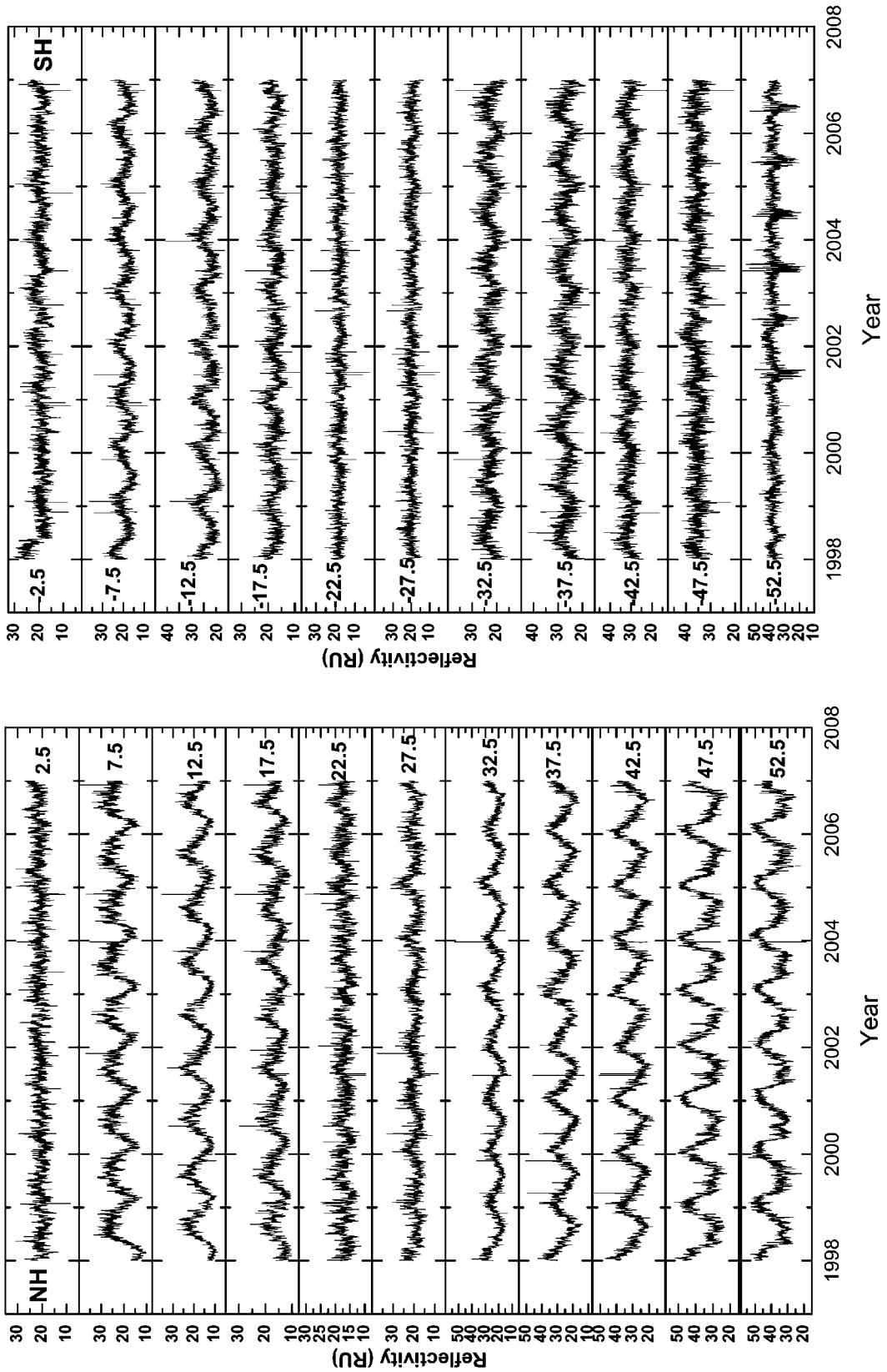

Figure 10. Zonal average reflectivity time series, 1998–2006, from the SeaWiFS 412 nm channel as a function of latitude from −55° to +55°. This figure is similar to one prepared for N7-TOMS [*Herman et al.*, 2001b].

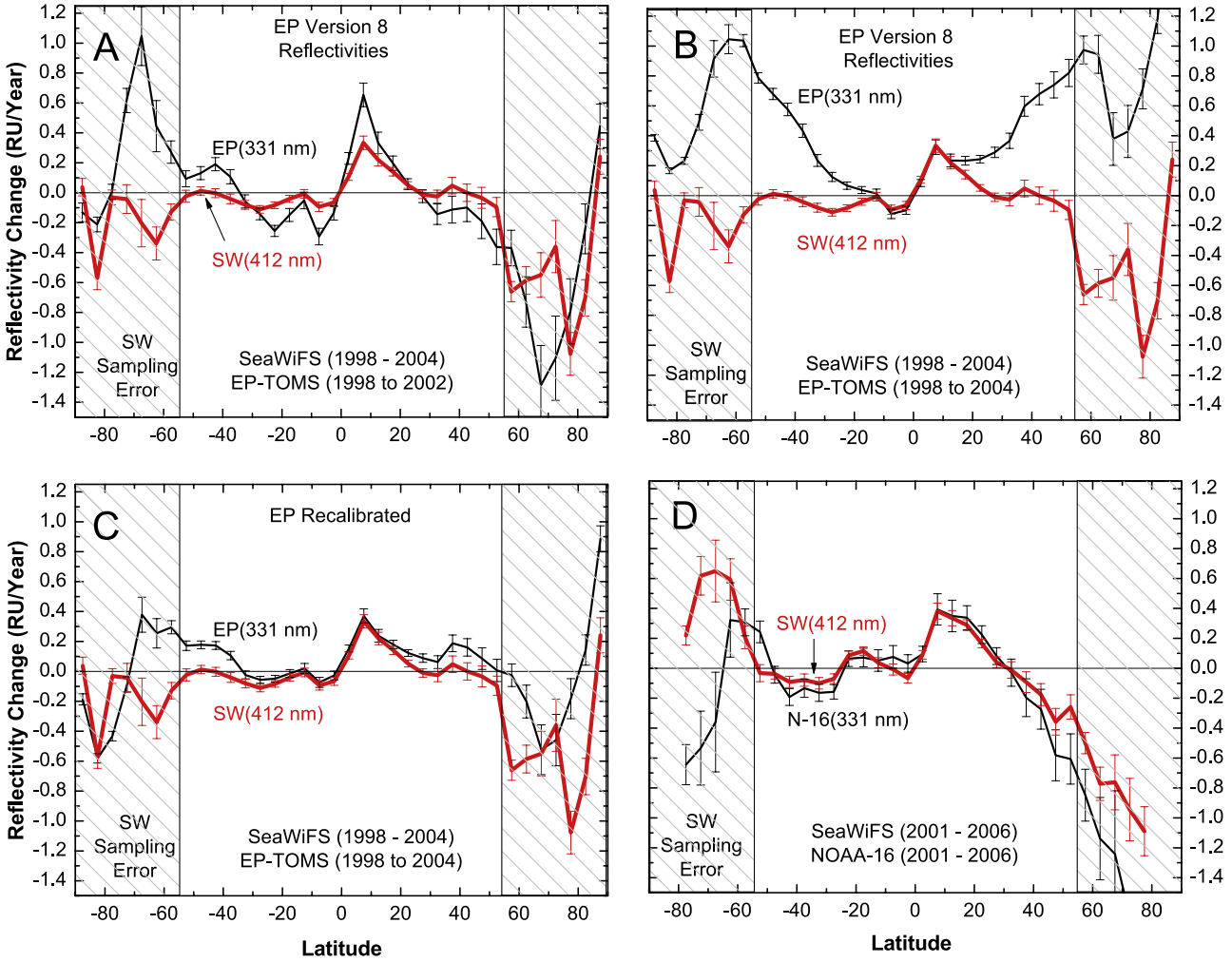

Figure 11. Reflectivity trends estimated from SW, EP, and N-16 using linear least squares fit to the reflectivity time series. (a) SW and EP (V8) 1998 to 2002, (b) SW and EP (V8) 1998 to 2004, (c) SW and EP (recalibrated), and (d) SW and N-16 2001 to 2006.

caused a net increase in cloud cover in response to a change in ocean currents.

5. Zonal Average Reflectivity Linear Trends (1998–2006)

5.1. EP and SW

[43] A comparison between EP and SW demonstrates why EP is not suitable for long-term reflectivity trend estimates. Five degree zonally averaged daily reflectivity time series for 85°S to 85°N are fit using linear least squares with the resulting slope (RU/year) shown in Figures 11a to 11d using SW as a reference data set. Figures 11a–11d are constructed using the same algorithm for SW, EP, and N-16 satellites, and are similar to the N7/TOMS figure appearing in the work of *Herman et al.* [2001b]. Figures 11a and 11b show the problems with EP Version-8 after 2002, and Figure 11c shows the improvement when the measured radiances were adjusted in the recently recalibrated EP data set using N-16 as a reference. Finally, Figure 11d shows the agreement between SW and N-16 that justifies the use of N-16 as a reference data set.

[44] The close agreement in Figure 11a between SW (1998–2006) and EP (1998–2002) in the latitude range between 35°S and 35°N shows that EP was radiometrically stable over the 1998 to 2002 period even though they differ in absolute calibration. Between 35° and 55° in both hemispheres, the linear trends estimated from SW and Version 8 EP start to diverge but are within 2σ error bars (Figure 11 shows 1σ error bars). Outside of the ±55° latitude range, SW has an incomplete data record because of a policy decision not to operate SW when the solar zenith angle is greater than 70°. This means that there is only summer SW data over the Antarctic ice sheet and over the Arctic. The result is a sampling error in the calculated SW slopes at high latitudes that prevents unbiased estimation of the annual linear trend at high latitudes. TOMS data are obtained for all daylight conditions regardless of zenith angle and form a better statistical sample (missing only dark winter months above the Artic and Antarctic circles) so that TOMS least squares annual-trend slopes should be valid to a latitude of ±70°. Poleward of 66.7° latitude, TOMS data have temporal sampling problems that are similar to those of SeaWiFS, which start at lower latitudes.

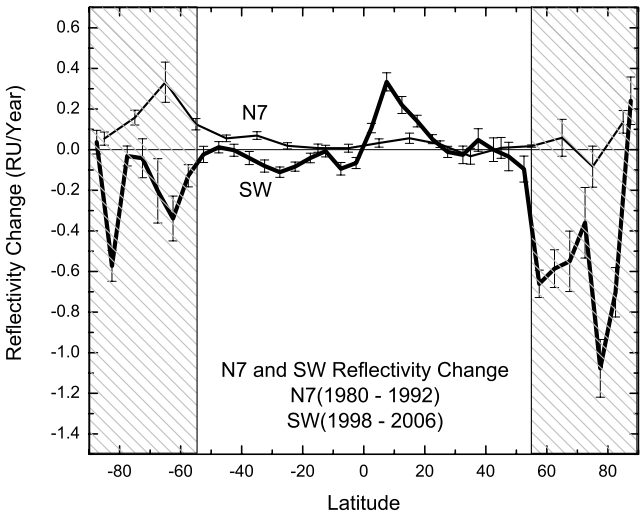

Figure 12. Reflectivity change observed by N7 from 1980 to 1992 and SW from 1998 to 2006. The N7 data have been taken from *Herman et al.* [2001b] with the addition of the shaded regions and a changed scale. The peak is at 7.5°N, representing a band from 5° to 10°.

[45] The most prominent trend feature in the EP (1998–2002) trend estimate is the statistically significant change observed in the band centered at 7.5°N with a maximum (0.5 RU/a) that appears to be driven by the El Nino-Southern Oscillation (ENSO) originating in the equatorial Pacific Ocean as a positive sea surface temperature (SST) anomaly in late 1996 to early 1997. This is a case of known changes in the ocean circulation and temperature affecting cloud cover over a sufficiently broad geographical region to affect zonal average trends. The results compare well with the SW trend estimate over a longer period (1998–2006).

[46] Extending Version 8 EP time series to 2004 shows the continuing calibration drift for EP at middle to high latitudes in both hemispheres (Figure 11b). If the Version-8 EP changes were correct, it would imply a major change in the total solar radiation reflected back to space since 1998, which is highly unlikely. The trends for SW show that the reflectivity data have remained approximately constant for most latitudes. The only place there seems to be zonal average trend of significance is in the latitude range from 2.5°N to 22.5°N with a peak at 7.5°N of 3.3 RU/decade. However, there are regional changes in reflectivity at midlatitudes that are discussed later.

[47] The most recent iteration of the EP calibration uses the better calibrated N-16 to adjust the EP measured radiances as a function of latitude and time for the period 2001 to 2004. The result is a much better agreement between EP and SW (Figure 11c). The new EP data are available on the TOMS website for reflectivity, ozone, aerosols, and UV irradiance.

[48] Figure 11d shows a direct comparison between the independent reflectivity data sets from SW and N-16 for the period 2001 to 2006. The estimated trends are nearly the same within 1σ error estimates between 55°N and 55°S where the temporal sampling errors are not present. The comparisons give confidence in the long term stability of both the SW and N-16 calibration over the 1998 to 2006 period.

5.2. N7 and SW

[49] When compared to the changes observed by N7 (Figure 12), the SW trends show some significant differences. Most prominent is the change at low latitudes that corresponds to the mid-Pacific Ocean ENSO region showing a strong increase in cloud cover. In the Southern Hemisphere midlatitudes N7 was showing a modest increase in reflectivity, while SW is showing a modest decrease. Since these represent different years, the changes may represent small, but real changes in cloud cover corresponding to the two periods 1980 to 1992 and 1998 to 2006.

[50] The reflectivity trends in Figure 12 can also be compared with Figures 1 and 2 from the study by *Norris* [2005], which analyzed the change in total cloud cover from ISCCP and EECRA data. The cloud cover from 1980 to 1992 shows, for 30°S to 30°N, almost no change over land for EECRA and -0.2 ± 0.07%/a change in cloud anomaly for ISCCP (1984–1993), and a change over oceans of 0.13 ± 0.01%/a change in cloud anomaly for EECRA data and -0.27 ± 0.06%/a for ISCCP data (1983–1993). The N7 reflectivity data shows a barely significant increase in reflectivity from 30°S to 30°N of about 0.03 ± 0.02 RU/a over both land and water, which is more in agreement with the EECRA data. ISCCP data continues to show a strong decrease after 1997 to 2000, in contradiction to both the EECRA data and to the SW reflectivity trend data (1998 to 2006).

6. Linear Time Series Trends Versus Latitude and Longitude (1998–2006)

[51] Analysis of reflectivity changes (mostly cloud reflectivity) as a function of latitude and longitude shows that there are distinct features from the N7 and SW derived reflectivity trends that are important for understanding likely changes in cloud cover that affects the amount of UV, VIS, and NIR radiation reaching the surface (Figure 13).

6.1. 1980–1992

[52] From Figure 13a based on N7 (1980 to 1992) Version 8 data, the major features show that there was a decrease in cloud cover in the western United States and Canada and in most of Europe with the strongest changes occurring above 40°N. There are also reflectivity decreases in eastern Russia between 50°N and 60°N. On a zonal average basis, these reflectivity decreases are offset to yield almost no net change. In contrast, the Southern Hemisphere shows a small net increase in zonal average reflectivity that is not offset by the regions of reflectivity decrease. Regions of cloud decrease occur over northern Australia, parts of Indonesia, South Africa, and Madagascar. This is especially the case for latitudes between 60°S and the Antarctic ice shelf where there appears to have been a significant increase in cloud cover. Since N7 cannot distinguish between clouds and ice, this increase could just as well be an increase in sea ice. However, as discussed previously [*Herman et al.*, 2001b], the sea ice during this period did not increase. Finally, there is the interesting feature that appears to be related to changes in the cold water Humboldt Current that

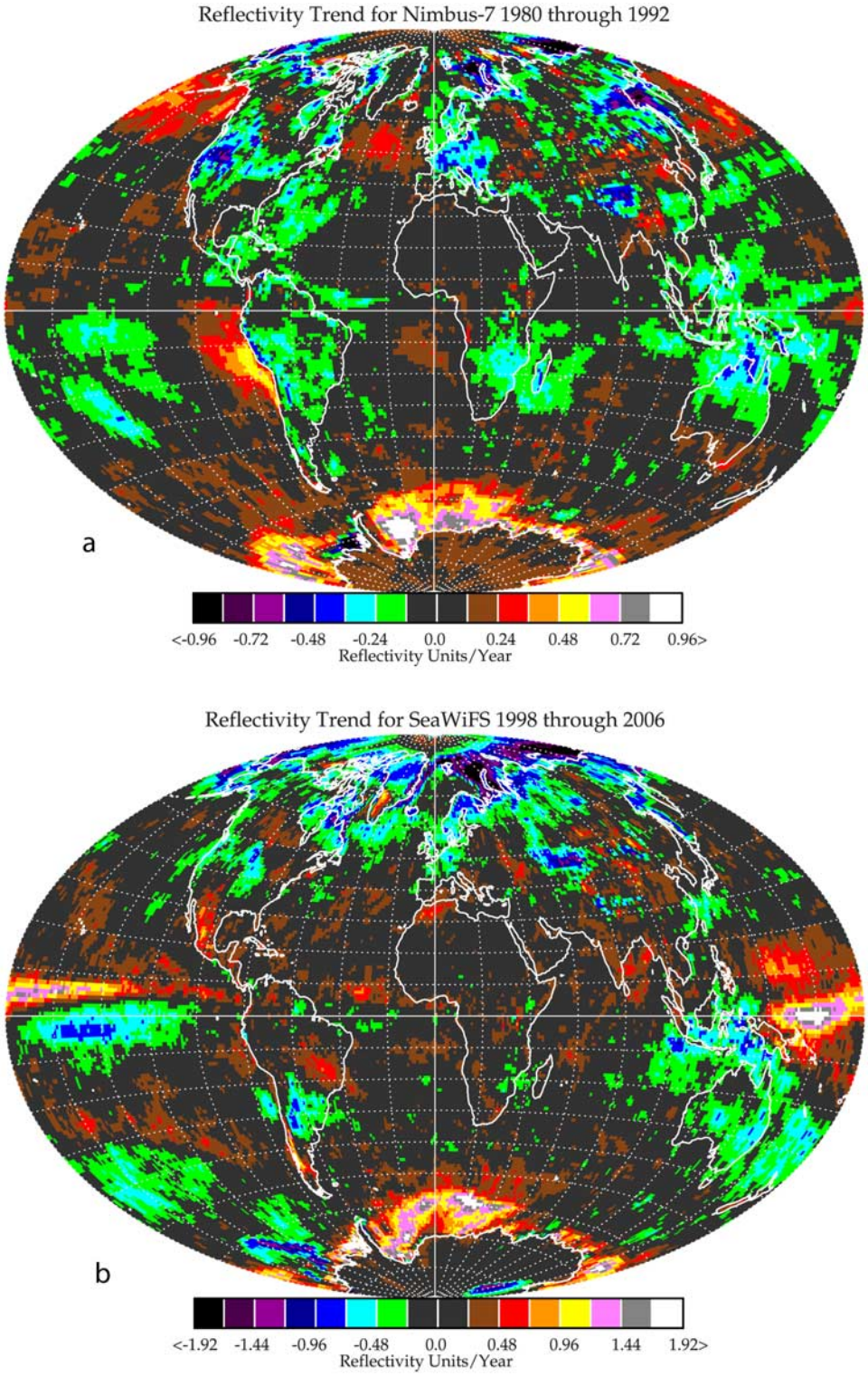

Figure 13. (a) N7 331 nm Version 8 reflectivity trends 1980 to 1992. (b) SW 412 nm reflectivity trends 1998 to 2006. For latitudes over 55°, the estimated trends for SW represent summer data sampling.

arises at high southern latitudes and reflects off of the western coast of South America. Changes in the current appear to have increased the amount of cloud cover in the region from 10°S to 30°S.

[53] Figures 13a and 13b are in agreement with the zonal averages in Figure 12 and with the EECRA data from *Norris* [2005] from 1980 to 2000. The EECRA data shows a small upward trend over the oceans, which may include

the ENSO effect that appears in the reflectivity data from SW.

6.2. 1998–2006

[54] Figure 13b shows the trends estimated for 1998 to 2006 obtained by using SW data. The dominant features are the strong reflectivity "increase-decrease dipole" located in the equatorial Pacific Ocean. The most prominent changes are (1) a decrease in the region between Northern Australia and Indonesia, and (2) the equatorial region decrease near 160°W and the large increase in reflectivity just north of the equator at 160°E and 160°W associated with the El Nino Southern Oscillation (ENSO). ENSO effects occur irregularly every few years accompanied by a weaker reversal usually 1 year later. While the aperiodic ENSO effect is felt in changing weather patterns over most of the globe, the largest effect on cloud reflectivity is near its ocean-current source in the equatorial Pacific Ocean. As shown in the zonal average data (Figure 12), the cloud increase in the 5°N–10°N band is not offset by the adjacent equatorial region of cloud decrease. The dipole was also present in EP observations from 1998 to 2002 (Figure 11a), but was largely absent in the earlier N7 period (Figures 12 and 13a).

[55] There are also reflectivity increases over land in a few places such as over the Indian Ocean, parts of Morocco and Algeria, northern Mexico/southern United States, and Canada. Similarly, there are decreases in reflectivity over central United States, northern Europe (60°N, 20°E), Kazakhstan (80°E 45°N), Argentina-Chile, and smaller decreases over Australia and New Zealand that produce corresponding increases in time-integrated solar irradiance (exposure) reaching the ground. While the decreasing cloud reflectivity increases solar radiation reaching the ground and total average exposure, changes in ozone are also important, since it affects UVB for clear-sky days when the irradiance is at a maximum for that day and location. Any decrease in cloud cover is especially important during the Southern Hemisphere summer where the total ozone amount is less and the Sun-Earth distance is smaller than for Northern Hemisphere summer. In Australia and other countries, any increase in UV exposure is especially detrimental to the European portion of the population, which has minimal natural UV protection (for skin cancer [*Diffey*, 1991] and a more general reference for health impact [*Lucas et al.*, 2006], eye cataracts [*Taylor*, 1990], suppression of the immune system [*Vermeer et al.*, 1991]), and to ecosystem biology [*Ghetti et al.*, 2006]. On the basis of the U.S. National Institutes of Health data, similar skin cancer problems are present in the United States, with more skin cancer occurring at lower latitudes where the UV exposure is higher. The seriousness of the very high UV exposure problem is observed in Australia, where skin cancer rates have increased dramatically (20% for basal cell, to 788 per 100,000 and over 90% for squamous cell, to 321 per 100,000 carcinomas) based on household surveys in 1985, 1990, and 1995 [*Staples et al.*, 1998]. This compares to the U.S. National Cancer Institute estimate of 14.5 per 100,000 for the United States. Skin cancer incidence by skin type has been estimated by the U.S. National Cancer Institute Surveillance, Epidemiology, and End Results (SEER) program, which states that Caucasian people have the highest melanoma incidence, followed by a much lower rate for Hispanics and African Americans, and with the lowest incidence for Asian Pacific islanders.

[56] At higher latitudes in the Northern Hemisphere, where there is much more cloud cover than in Australia (e.g., central Europe 50°N, northern United States, and Canada), a small decrease in cloud cover and ozone may produce the beneficial effect of increasing natural vitamin D production from increased UVB (280 to 315 nm) exposure during spring and summer months [*Grant*, 2002; *Holick*, 2004] without producing greatly enhanced rates of skin cancer.

[57] As during the N7 operating period, SW reflectivity shows a continued increase in reflectivity in the region near and east of the Antarctica Peninsula, part of which may be caused by increases of floating sea ice [*Stammerjohn et al.*, 2008; *Fetterer et al.*, 2008] (http://nsidc.org/data/seaice_index/). Reflectivity changes observed by SW at high latitudes are only representative of data obtained near summer solstice when the solar zenith angle was less than 70°.

[58] Since the summer months are the period when the maximum solar irradiance reaches the Earth's surface, changes in early summer (May to June in the Northern Hemisphere and November to December in the Southern Hemisphere) cloud reflectivity (Figure 14) will have the maximum effect on human health and plant productivity from changes in UV exposure. The noise level is higher in the summer trend estimate, since there are fewer data points (1/6) compared to the annual data. Because of this, only positive and negative changes greater than 0.75 RU/year (blue and orange) should be considered as significant in Figure 14.

[59] For example, there is still a decrease in cloudiness over Australia, but the region of reduced cloud cover now covers the coastal regions where the bulk of the population lives. The data in Figure 14 show a significant increase in cloudiness over north central Russia (60°N to 70°N and 80°E to 100°E) that is only weakly present in the annual data. The reflectivity decreases over the northwestern United States and southwestern Canada is present in both the annual and summer trends. There are bands of decrease off of the U.S. west coast that stretches across the northern Pacific and in the southern Pacific and increase on the United States east coast from 40°N to 50°N. There are also two bands of increased reflectivity (increased cloud cover) in the low-latitude SH Pacific and near the equator, with the largest increases from 170°E to 170°W.

7. Summary

[60] This paper examines and compares the long-term changes that have occurred in the available UV (331 nm) and Blue (412 nm) wavelength reflectivity time series that were obtained from two satellite instruments. The first was Nimbus-7/TOMS (1979 to 1992), launched in November 1978, recalibrated in 1986, and again, every few years, using the latest algorithms and in-flight data. The second was SeaWiFS (1998 to 2007), which has been recalibrated and reprocessed during its lifetime using in-flight data. The Version-8 data processing was used for N7, EP, and OMI. For EP the independent in-flight calibration has now been replaced with a calibration tied closely to N-16, which partially corrects some of the calibration problems associ-

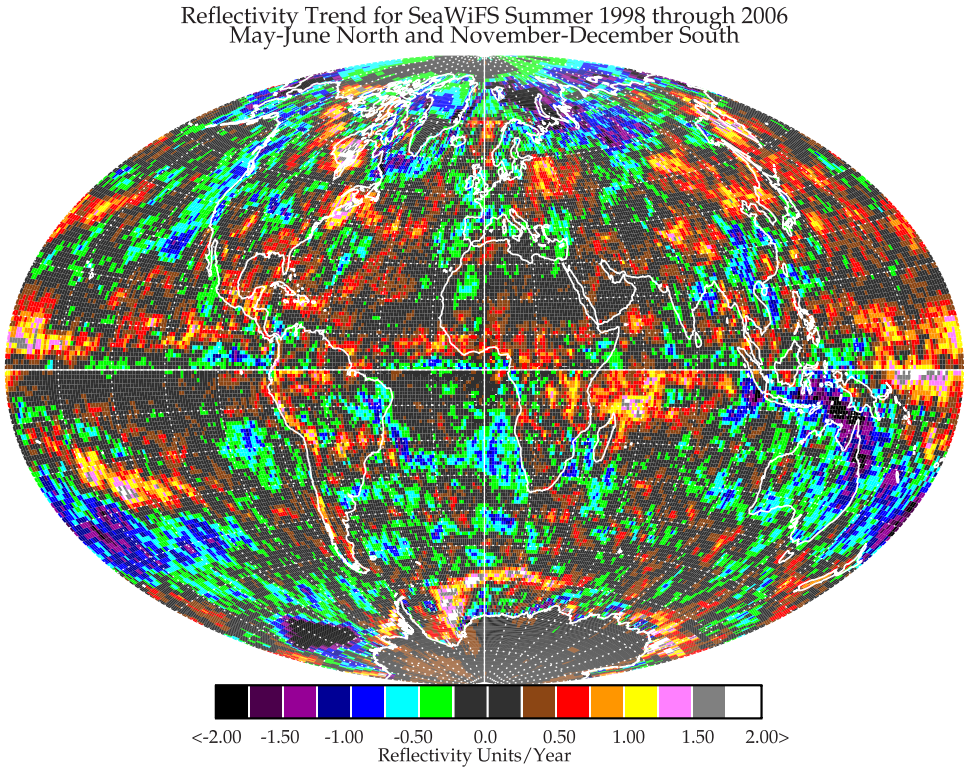

Figure 14. Reflectivity trends from SeaWiFS 412 nm radiances for 1998 to 2006 during May and June in the Northern Hemisphere and during November and December in the Southern Hemisphere. For the summer, there is data at latitudes up to 85° during the entire 2-month period. Note that the Arctic and Antarctic ice sheets now show no significant changes in reflectivity indicating a very stable instrument calibration. Note that the data are split at the equator.

ated with EP Version 8. However, while EP reflectivities are improved, they should not be used for trend estimations.

[61] The NOAA SBUV-2 series were examined for their potential to fill in gaps between N7 and SW, but they show calibration differences as a function of latitude that have to be resolved before the combined data can be used for global trend analysis. In the, 37.5°N and 37.5°S bands the calibration differences are small and the data sets are shown to be well correlated. The correlation between overlapping independent reflectivity time series gives confidence that the short-term variations are geophysical and not instrument artifacts.

[62] We have separately processed SeaWiFS radiance data to produce an equivalent to the TOMS reflectivity data set, but at 412 nm. We have compared N7, EP, SW, and OMI reflectivity data sets and found fairly close agreement on a zonal average basis, except in the equatorial region where there has been a stronger ENSO effect during the 1998–2007 period than during the previous N7 period of 1980–1992. We had to use SW instead of EP to extend the time series to 2007, since the independent in-flight calibration of EP drifted after 2002. The resulting SW trend analysis shows a strong increase in reflectivity in the equatorial region indicating that there has been additional net cloud formation produced by changes in the underlying ocean currents. An analysis of changes that have occurred as a function of latitude and longitude show that there are regional reflectivity decreases in parts of Europe that are accompanied by increases in the southwest United States and parts of Mexico. The most dominant feature is the reflectivity "dipole" observed in the equatorial Pacific Ocean caused by the ENSO effect, which causes a net increase in zonal average reflectivity. For most of the rest of the Earth, there have been only small changes that are not statistically significant in the SW reflectivity analysis. The long-term trends in N7 and SW reflectivity appear to be in agreement with Norris' EECRA cloud analysis, but in disagreement with the ISCCP long-term cloud cover trend. When comparing reflectivity data from N7 to that from SW, the fractional occurrence (fraction of days) of high reflectivity values over Hudson Bay, Canada (snow/ice and clouds) appears to have decreased when comparing reflectivity data from 1980 to 1992 to 1997–2007, suggesting shorter duration of ice in Hudson Bay since 1980.

Appendix A: Stokes Derivation of $C_T = (1 - R)/(1 - R_G)$

[63] Assume that the cloud-ground system can be approximated by a two-layer Stokes problem with atmospheric effects neglected. Assume that the clouds have different transmission and reflection properties for diffuse T_D, R_D

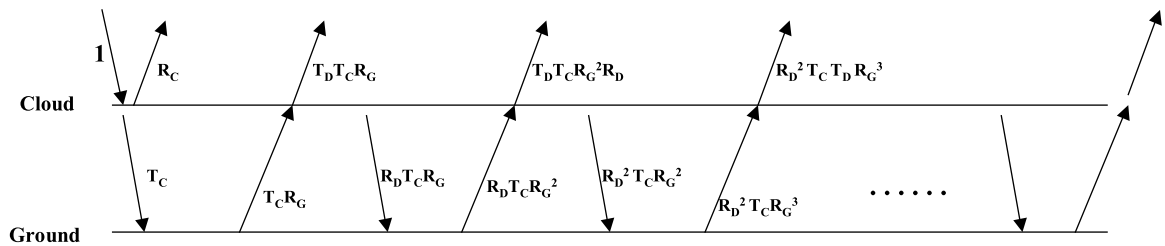

$$R_{SYSTEM} = R_C + R_G T_C T_D [\, 1 + R_G R_D + (R_G R_D)^2 + \ldots..] = R_C + R_G T_D T_C / [1 - R_G R_D] \quad (1)$$

$$C_T = T_C [\, 1 + R_G R_D + (R_G R_D)^2 + \ldots..] = T_C / [1 - R_G R_D] \quad (2)$$

Using equation (2), rewrite (1) as

$$1 - R_{SYSTEM} = 1 - R_C - R_G T_D T_C / [1 - R_G R_D] = 1 - R_C - R_G T_D C_T \quad (3)$$

Assume $T_C = 1 - R_C$ and $T_D = 1 - R_D$ Rewrite (2) as $C_T [1 - R_G R_D] = 1 - R_C$

Now (3) becomes $1 - R_{SYSTEM} = C_T [1 - R_G R_D] - R_G C_T [\, 1 - R_D] = C_T [\, 1 - R_G] \quad (4)$

Finally,

$$\boxed{C_T = [1 - R_{SYSTEM}] / [\, 1 - R_G]}$$

R_G = Reflectivity of the Ground R_C = Direct beam cloud reflectivity R_D = Diffuse flux cloud reflectivity

R_{SYSTEM} = Reflectivity of the combined ground-cloud system

T_C and T_D are the corresponding cloud transmissivities

Assume R_{SYSTEM} = LER as an approximation to the reflectivity seen by the satellite.

Figure A1. Stokes diagram for CT for unit irradiance incident on a cloud of transmittance TC over a surface of reflectance RG. The cloud and surface have diffuse transmittance and reflectivity of TD and RD.

and direct-Sun T_C, R_C. The arrows in Figure A1 represent the partial contributions to the upward and downward fluxes.

References

Bago, E. P. (2002), Solar activity, cloud cover, and climate change, Ph.D. thesis, Armagh Obs., Armagh, U. K.

Barnes, R. A., and A. W. Holmes (1993), Overview of the SeaWiFS ocean sensor, *Proc. SPIE*, *1939*, 224–232, doi:10.1117/12.152849.

Barnes, R. A., E.-N. Yeh, and R. E. Eplee (1996), SeaWiFS calibration topics, Part 1, *NASA Tech. Memo., 104566*, 39.

Cornwell, A. R., W. A. Gough, and L. J. S. Tsuji (2004), Trends in seasonal sea ice duration in southwestern Hudson Bay, *Arctic*, *54*(2), 142–148.

Croke, M. S., R. D. Cess, and S. Hameed (1999), Regional cloud cover change associated with global climate change: Case studies for three regions of the United Stated, *J. Clim.*, *12*, 2128–2134.

Diffey, B. L. (1991), Solar ultraviolet radiation effects on biological systems, *Rev. Phys. Medicine Biol.*, *36*(3), 299–328.

Eck, T. F., P. K. Bhartia, P. H. Hwang, and L. L. Stowe (1987), Reflectivity of Earth's surface and clouds in ultraviolet from satellite observations, *J. Geophys. Res.*, *92*, 4287–4296, doi:10.1029/JD092iD04p04287.

Eck, T. F., P. K. Bhartia, and J. B. Kerr (1995), Satellite estimation of spectral UVB irradiance using TOMS derived total ozone and UV reflectivity, *Geophys. Res. Lett.*, *22*, 611–614, doi:10.1029/95GL00111.

Eplee, R. E., W. D. Robinson, S. W. Bailey, D. K. Clark, P. J. Werdell, M. Wang, R. A. Barnes, and C. R. McClain (2001), Calibration of SeaWiFS. II. Vicarious techniques, *Appl. Opt.*, *40*, 6701–6718, doi:10.1364/AO.40.006701.

Evan, A. T., A. K. Heidinger, and D. J. Vimont (2007), Arguments against a physical long-term trend in global ISCCP cloud amounts, *Geophys. Res. Lett.*, *34*, L04701, doi:10.1029/2006GL028083.

Fetterer, F., K. Knowles, W. Meier, and M. Savoie (2008), Sea ice index, Natl. Snow and Ice Data Cent., Boulder, Colo.

Ghetti, F., G. Checcucci, and J. Bornman (Eds.) (2006), *Environmental UV Radiation: Impact on Ecosystems and Human Health and Predictive Models, Proceedings of the NATO Advanced Study Institute on Environmental UV Radiation*, vol. 57, Springer, Dordrecht, Netherlands.

Grant, W. B. (2002), An estimate of premature cancer mortality in the U.S. due to inadequate doses of solar ultraviolet-B radiation, *Cancer*, *94*(6), 1867–1875, doi:10.1002/cncr.10427.

Hahn, C. J., and S. G. Warren (1999), Extended edited synoptic cloud reports from ships and land stations over the globe, 1952–1996, NDP026C, 71 pp., Carbon Dioxide Inf. Anal. Cent., Oak Ridge Natl. Lab, Oak Ridge, Tenn.

Hatzianastassiou, N., C. Matsoukas, A. Fotiadi, K. G. Pavlakis, E. Drakakis, D. Hatzidimitriou, and I. Vardavas (2005), Global distribution of Earth's surface shortwave radiation budget, *Atmos. Chem. Phys.*, *5*, 2847–2867.

Herman, J. R., and E. A. Celarier (1997), Earth surface reflectivity climatology at 340 nm to 380 nm from TOMS data, *J. Geophys. Res.*, *102*, 28,003–28,011, doi:10.1029/97JD02074.

Herman, J. R., R. Hudson, R. McPeters, R. Stolarski, Z. Ahmad, X.-Y. Gu, S. Taylor, and C. Wellemeyer (1991a), A new self-calibration method applied to TOMS/SBUV backscattered ultraviolet data to determine long term global ozone change, *J. Geophys. Res.*, *96*, 7531–7545, doi:10.1029/90JD02662.

Herman, J. R., R. Hudson, R. McPeters, R. Stolarski, and Z. Ahmad (1991b), Global average ozone change from October 1978 to May 1990, *J. Geophys. Res.*, *96*, 17,297–17,305, doi:10.1029/91JD01553.

Herman, J. R., P. K. Bhartia, J. Ziemke, Z. Ahmad, and D. Larko (1996), UV-B increases (1979–1992) from decreases on total ozone, *Geophys. Res. Lett.*, *23*, 2117–2120, doi:10.1029/96GL01958.

Herman, J. R., N. Krotkov, E. Celarier, D. Larko, and G. Labow (1999), The distribution of UV radiation at the Earth's surface from TOMS measured UV-backscattered radiances, *J. Geophys. Res.*, *104*, 12,059–12,076, doi:10.1029/1999JD900062.

Herman, J. R., R. D. Piacentini, J. Ziemke, E. Celarier, and D. Larko (2000), Interannual variability of ozone and UVB ultraviolet exposure, *J. Geophys. Res.*, *105*, 29,189–29,194, doi:10.1029/2000JD900524.

Herman, J. R., E. Celarier, and D. Larko (2001a), UV 380 nm reflectivity of the Earth's surface, clouds, and aerosols, *J. Geophys. Res.*, *106*, 5335–5351, doi:10.1029/2000JD900584.

Herman, J. R., D. Larko, E. Celarier, and J. Ziemke (2001b), Changes in the Earth's UV reflectivity from the surface, clouds, and aerosols, *J. Geophys. Res.*, *106*, 5353–5369, doi:10.1029/2000JD900435.

Holick, M. F. (2004), Sunlight and vitamin D for bone health and prevention of autoimmune diseases, cancers, and cardiovascular disease, *Am. J. Clin. Nutrition*, *80*(6), 1678S–1688S.

Hollandsworth, S. M., R. D. McPeters, L. E. Flynn, W. Planet, A. J. Miller, and S. Chandra (1995), Ozone trends deduced from combined Nimbus 7 SBUV and NOAA 11 SBUV/2 data, *Geophys. Res. Lett.*, *22*, 905–908, doi:10.1029/95GL00605.

Krotkov, N. A., J. R. Herman, P. K. Bhartia, Z. Ahmad, and V. Fioletov (2001), Satellite estimation of spectral surface UV irradiance: 2. Effect of horizontally homogeneous clouds, *J. Geophys. Res.*, *106*, 11,743–11,759.

Lubin, D., E. H. Jensen, and H. P. Gies (1998), Global surface ultraviolet radiation climatology from TOMS and ERBE data, *J. Geophys. Res.*, *103*, 26,061–26,092, doi:10.1029/98JD02308.

Lucas, R., T. McMichael, W. Smith, and B. Armstrong (2006), Solar ultraviolet radiation: Global burden of disease from solar ultraviolet radiation, *Rep. 13*, World Health Org., Geneva.

McPeters, R. D., S. M. Hollandsworth, L. E. Flynn, J. R. Herman, and C. J. Seftor (1996), Long-term ozone trends derived from the 16-year combined Nimbus 7 - Meteor 3 TOMS Version 7 record, *Geophys. Res. Lett.*, *23*, 3699–3702, doi:10.1029/96GL03540.

Morel, A., and L. Prieur (1977), Analysis of variations in ocean color, *Limnol. Oceanogr.*, *22*, 709–722.

Norris, J. R. (2005), Multidecadal changes in near-global cloud cover and estimated cloud cover radiative forcing, *J. Geophys. Res.*, *110*, D08206, doi:10.1029/2004JD005600.

Rossow, W. B., and R. A. Schiffer (1991), ISCCP cloud data products, *Bull. Am. Meteorol. Soc.*, *72*, 2–20, doi:10.1175/1520-0477(1991)072<0002:ICDP>2.0.CO;2.

Smith, N. R. (1995), 1995: An improved system for tropical ocean subsurface temperature analyses, *J. Atmos. Oceanic Technol.*, *12*, 850–870, doi:10.1175/1520-0426(1995)012<0850:AISFTO>2.0.CO;2.

Somerville, R. C. J., and L. A. Remer (1984), Cloud optical thickness feedback in the CO_2 climate problem, *J. Geophys. Res.*, *89*, 9668–9672, doi:10.1029/JD089iD06p09668.

Stammerjohn, S. E., D. G. Martinson, R. C. Smith, X. Yuan, and D. Rind (2008), Trends in Antarctic annual sea ice retreat and advance and their relation to El Nino-Southern Oscillation and Southern Annular Mode variability, *J. Geophys. Res.*, *113*, C03S90, doi:10.1029/2007JC004269.

Staples, G., R. Marks, and G. Giles (1998), 1998 Trends in the incidence of non-melanocytic skin cancer (NMSC) treated in Australia 1985–1995: Are primary prevention programs starting to have an effect, *Int. J. Cancer*, *78*, 144–148, doi:10.1002/(SICI)1097-0215(19981005)78:2<144::AID-IJC3>3.0.CO;2-Z.

Stolarski, R. S., R. D. McPeters, and J. R. Herman (1991), Total ozone trends deduced from Nimbus 7 TOMS data, *Geophys. Res. Lett.*, *18*, 1015–1018, doi:10.1029/91GL01302.

Sun, B., P. Y. Groisman, R. S. Bradley, and F. T. Keimig (2000), Temporal changes in the observed relationship between cloud cover and surface air temperature, *J. Clim.*, *24*, 4341–4357.

Surabi Menon, S., J. Hansen, L. Nazarenko, and Y. Luo (2002), Climate effects of black carbon aerosols in China and India, *Science*, *27*, 2250–2253.

Taylor, H. R. (1990), Cataracts and ultraviolet light, in *Global Atmospheric Change and Public Health*, edited by J. C. White, pp. 61–65, Elsevier Sci., New York.

Tselioudis, G., W. B. Rossow, and D. Rind (1992), Global patterns of cloud optical thickness variation with temperature, *J. Clim.*, *5*, 1484–1495, doi:10.1175/1520-0442(1992)005<1484:GPOCOT>2.0.CO;2.

Vasilkov, A., N. Krotkov, J. Herman, C. McClain, K. Arrigo, and W. Robinson (2001), Global mapping of underwater UV fluxes and DNA-weighted exposures using TOMS and SeaWifs data products, *J. Geophys. Res.*, *106*(C11), 27,205–27,219, doi:10.1029/2000JC000373.

Vasilkov, A. P., J. Herman, N. A. Krotkov, B. G. Mitchell, and M. Kahru (2002), Problems in assessment of the UV penetration into natural waters from space-based measurements, *Opt. Eng.*, *41*, 3019–3027, doi:10.1117/1.1516822.

Vasilkov, A. P., J. R. Herman, Z. Ahmad, M. Kahru, and G. Mitchell (2005), Assessment of the ultraviolet radiation field in ocean waters from space-based measurements and full radiative transfer calculations, *Appl. Opt.*, *44*, 2863–2869, doi:10.1364/AO.44.002863.

Vermeer, M., G. J. Schmieder, T. Yoshikawa, J.-W. van den Berg, M. S. Metzman, J. R. Taylor, and J. W. Streilein (1991), Effects of ultraviolet B light on cutaneous immune responses of humans with deeply pigmented skin, *J. Invest. Dermatol.*, *97*, 729–734, doi:10.1111/1523-1747.ep12484259.

J. R. Herman and N. C. Hsu, NASA Goddard Space Flight Center, Greenbelt, MD 20771, USA. (jay.r.herman@nasa.gov)

G. Labow and D. Larko, Science Systems and Applications, Inc., Lanham, MD 20706, USA.